Title
Electrical Transport Spectroscopy (ETS) for In Situ Probing Electrode-Electrolyte Interfaces

Author
Zhong, Guangyan

Publication Date
2021

Peer reviewed|Thesis/dissertation

UNIVERSITY OF CALIFORNIA

Los Angeles

Electrical Transport Spectroscopy (ETS) for In Situ Probing Electrode-Electrolyte Interfaces

A dissertation submitted in partial satisfaction of the

requirements for the degree Doctor of Philosophy

in Chemistry

by

Guangyan Zhong

2021

ABSTRACT OF THE DISSERTATION

Electrical Transport Spectroscopy (ETS) for In Situ Probing Electrode-Electrolyte Interfaces

by

Guangyan Zhong

Doctor of Philosophy in Chemistry

University of California, Los Angeles, 2021

Professor Xiangfeng Duan, Chair

Electrochemistry of metallic nanostructures has played an essential role in a wide range of energy-related technologies. A fundamental understanding of the electrocatalytic surface is crucial for developing future generations of electrocatalysts with improved catalytic activity. Various spectroscopy-based methods have been applied in electrochemical surface studies, but most of these techniques are limited to ex-situ studies. In situ monitoring of catalytic interface during the electrochemical process is considered most informative yet extremely challenging. The fact that electrochemical interfaces are buried between the solid electrode and liquid electrolyte makes them difficult to access by traditional spectroscopic method. Methods that are able to circumvent these challenges often require unusual device design or highly complicated facilities.

Our group specifically designed Electrical transport spectroscopy (ETS) for in situ monitor of electrochemical interfaces. When the dimension of a metallic structure decreases to the mean free path of the electrons within it, the diffusive scattering induced by the surface adsorbates can

produce a significant change in resistivity. During an electrochemical cycle, the specifixally adsorbed molecules on the nanocatalysts surface could produce a detectable conductance change, providing an effective signaling pathway for in situ probing different molecular species at the electrode-electrolyte interface during the electrochemical process. With this novel nanoelectronic measurement approach, we can conduct a series of systematic investigations of nano-electrocatalysts surface chemistry for a wide range of fundamentally or practically important electrocatalytic reactions.

In this thesis, I will present three examples utilizing ETS for the in-situ characterization of the electrode-electrolyte interfaces. First, we investigated competitive anionic chemisorption on the platinum surface and its relationship with ORR kinetics on Pt (**Chapter 2**). Nest, we acquired ETS results under controlled potential range in a serials of pH conditions, which allows to determine the pKa of hydronium adsorbed on the platinum surface for interpreting distinct hydrogen evolution reaction kinetics at different pH (**Chapter 3**). Lastly, we explored the ETS approach sensing applciations including their potential for the detection of hydrogen peroxide and DNA molecules (**Chapter 4**).

The dissertation of Guangyan Zhong is approved.

Anastassia Alexandrova

Alexander Spokoyny

Yu Huang

Xiangfeng Duan, Committee Chair

University of California, Los Angeles

2021

Table of Contents

List of Figures

ACKNOWLEDGEMENTS

First and foremost, I would like to express my deepest gratitude to Prof. Xiangfeng Duan and Prof. Yu Huang. Over the five years of Ph.D. study, you supported me to continuously move on with your patience, knowledge, and dedication to scientific research. I can always learn something new through each informative discussion of my research project with you two. Your enthusiasm to work and strong willingness of learning will always urge me to keep a positive attitude in the future. Besides, I would also like to thank Prof. Anastassia Alexandrova and Prof. Alexander Spokoyny, for their helpful comment and continuous encouragement. Special thanks go to the Graduate Office of UCLA Chemistry and Biochemistry, for their kind assistance in all the general affairs over the five years.

I am eternally grateful to all my lab mates from the chemistry department and MSE department: Mengning, Zhihong, Peiqi, Yiliu, Chengzhang, Yuan, Jian, Zhaoyang, Haotian, Jin, Dong, Mufan, Frank, Dan, Daniel, Bocheng, Wang, Xiaoyang, Lele, Huilong, Rongli, Sibo, Zeyan, Jin, Yun-Chiao, Huiying, Michelle, Choi, Sungjeon, Hao, Ao, Yang, Huaying, Jingyuan, Daowei, Chuancheng, Enbo and Zipeng. You guys not only provide experimental support but also create a super friendly atmosphere within the research group. I would also like to thank my roommate Chen, Zhiyu for keeping me accompanied in my Ph.D. life at UCLA. Special thanks go to Jiadong, Ian, Yunke, and Lydia, for your constant caring and support transmitted across the Pacific Ocean.

Last but not least, I would like to thank my family, especially my parents. Thank you for raising me in a positive environment and encouraging me to pursue what I'm aiming at. Thank you for forging me into an independent and optimistic young man. I wouldn't have finished this journey without the unselfish love and wholehearted support from you two, I love you.

COPYRIGHT AND CO-AUTHOR CONTRIBUTION

I would like to express my gratitude to AAAS, John Wiley and Sons, and Springer Nature for granting the permission to reprint several figures in **Chapter 1** and **Chapter 4**.

Chapter 2 is a version of :

Authors: Mengning Ding, Guangyan Zhong, Zipeng Zhao, Zhihong Huang, Mufan Li, Hui-Ying Shiu, Yuan Liu, Imran Shakir, Yu Huang, and Xiangfeng Duan.

Title: On-Chip in Situ Monitoring of Competitive Interfacial Anionic Chemisorption as a Descriptor for Oxygen Reduction Kinetics.

Journal: *ACS Central Science*; Year: 2018; Volume: 4; Page: 590-599.

Mengning Ding, Xiangfeng Duan, and Yu Huang designed the research; Mengning Ding, Guangyan Zhong, Zipeng Zhao, Zhihong Huang, Mufan Li, Hui-ying Shiu, and Yuan Liu performed the research, Mengning Ding, Guangyan Zhong, Xiangfeng Duan, and Yu Huang analyzed the data, and Mengning Ding, Xiangfeng Duan, and Yu Huang wrote the paper.

Chapter 3 is a version of :

Authors: Guangyan Zhong, Tao Cheng, Zhihong Huang, Chengzhang Wan, Aamir Shah, Sibo Wang, William A. Goddard III, Yu Huang, Xiangfeng Duan.

Title: Platinum Surface Hydronium pKa and Its Impact on Hydrogen Evolution Reaction.

Status: In preparation for publication.

Guangyan Zhong, Tao Cheng, Xiangfeng Duan, Yu Huang, and William A. Goddard III designed the research; Guangyan Zhong, Zhihong Huang, Chengzhang Wan, Aamir Shah, Sibo Wang performed the experimental part of the research; Tao Cheng performed the simulation part of the research; Guangyan Zhong, Tao Cheng, Xiangfeng Duan, Yu Huang, and William A. Goddard III analyzed the data and wrote the paper.

VITA

Guangyan Zhong received his B.S. degree in Chemistry from Peking University, Beijing, China in 2016. He joined Professor Dahui Zhao's group at Peking University in 2014 as an undergraduate researcher and worked on the synthesis of the synthesis of oligoethynylfluorene substituted triscyclometalated iridium complex. After that, he joined Professor Xiangfeng Duan's group at UCLA in 2016 and conducted research related to the solution-catalyst interface based on electrical transport spectroscopy. He was awarded UCLA Chemistry and Biochemistry Excellence in Research Fellowship in the year 2020 and Dr. Myung Ki Hong Dissertation Award in the year 2021.

Chapter 1. Introduction and background

1. Electrochemistry at the electrode-electrolyte interface

Electrocatalysis is a central part of research and development in energy conversion technologies[1]. For instance, the electrochemistry reaction catalyzed by platinum and other transition metal is critical in a wide range of energy-related technologies, including fuel cells, batteries, and many other electro-/photocatalytic processes (**Figure 1-1**)[2-5].

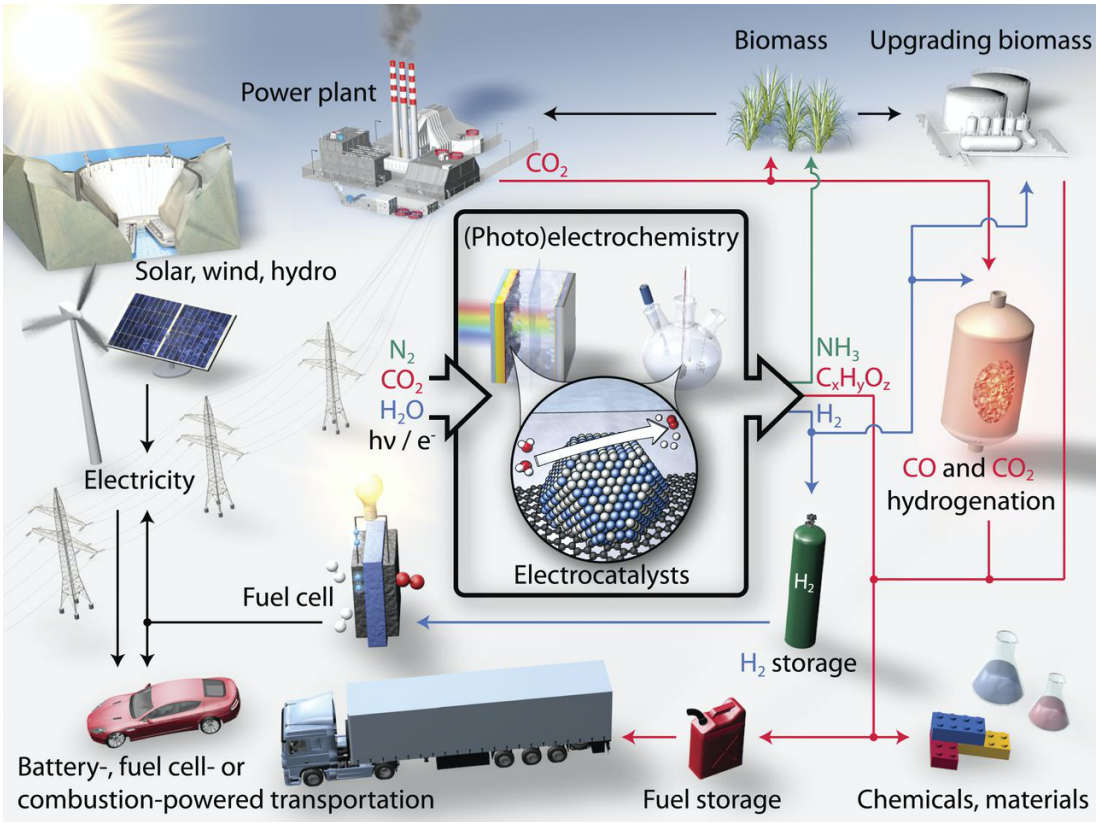

Figure 1-1. The central role of electrocatalysis in a sustainable energy future. Adapted from reference 1, reprinted with permission from AAAS.

The electrochemical interface is the focal point where key components, i.e., chemicals, ions, and electrons, of electrochemical reactions converge, interact and diverge. A fundamental understanding of the molecular structures of the electrochemical interfaces and their role in governing the heterogeneous electrocatalytic reaction rates are essential for developing future

generations of electrocatalysts with improved catalytic activity and stability for variable relevant electrochemical reactions, including hydrogen evolution reactions (HER) and oxygen reduction reaction (ORR)[6, 7]. To this end, various *in situ* characterizations, including X-ray based spectroscopy as well as vibrational spectroscopies including Fourier transform infrared (FTIR), sum-frequency generation (SFG), and Raman spectroscopy[8-14], and advanced simulations have been developed for probing and understanding the complex interfacial molecular structures of electrode/electrolyte interfaces. The next part will be a brief description of various techniques applicable to solid/liquid interfacial study.

2. Current in-situ characterization of electrode-electrolyte interface.

Compared to the investigation of a single surface, the solid/liquid interface study is posing an even greater challenge to the field of surface science. Techniques including electron microscopy, low-energy electron diffraction (LEED), and X-ray photoelectron spectroscopy (XPS), which are powerful tools for analyzing the surface structure and electronic state in high vacuum, cannot be applied to solid/liquid interfaces due to the presence of liquid.

Despite extreme technical complexity, various characterization methods have been developed to unravel the structure of solid/liquid interfaces. Techniques such as nonlinear spectroscopy, Raman spectroscopy, and synchrotron-radiation-based X-ray techniques are suitable for the investigation of metal surfaces in solution (summarized in **Table 1-1**). What's more, incorporation of potentiostat and reference electrode with the aforementioned techniques has made it possible for in situ or in operando characterizations for electrode/electrolyte interface. The revealed structure information and chemical details at the interface during active reaction cycles are essential for establishing a fundamental basis and guiding the rational design of highly active and long-lasting catalysts.

Table 1-1. Techniques available for in situ evaluation of electrode/electrolyte interface

Technique name	Abbreviation	Available information	Limitation
Synchrotron X-ray absorption spectroscopy	XAS XANES, EXAFS	Oxidation state, neighboring atomic species, bond distances, coordination number	Require standard sample, signal not only originated from surface
IR reflection absorption spectroscopy	IRRAS, RAIRS SNIFTIRS	Bonding information of molecules at the interface	Limited mass transfer, large solution resistance
Attenuated total reflection IR spectroscopy	ATR-IRS ATR-SEIRAS	Bonding information of molecules at the interface	Unable to analyze single crystal surface
Sum frequency generation spectroscopy	SFG	Bonding information of molecules at the interface	Complicated apparatus and data analysis
Surface enhanced Raman scattering	SERS SHINERS	Bonding information of molecules at the interface	Limited material type
Electrochemical quartz crystal microbalance	EQCM, EQCN	Mass of adsorbed species at the surface	Mass change observed may be rationalized in different combinations

2.1 Synchrotron radiation source based X-ray absorption spectroscopy

Due to limited absorption by water, X-ray is considered to be ideal radiation for the analysis of electrode/electrolyte interfaces. However, the examination of interfacial structure with an ideal signal-to-noise ratio is not possible before the development of synchrotron radiation that has high brilliance and directionality[15]. Among these techniques, the X-ray absorption fine structure (XAFS) is more commonly used because its target is not limited to crystalline solid surfaces like surface X-ray scattering. XAFS is obtained by monitoring the absorption of X-ray by the sample. It includes the X-ray absorption near-edge structure (XANES) and the extended X-ray absorption fine structure (EXAFS) (**Figure 1-2**).

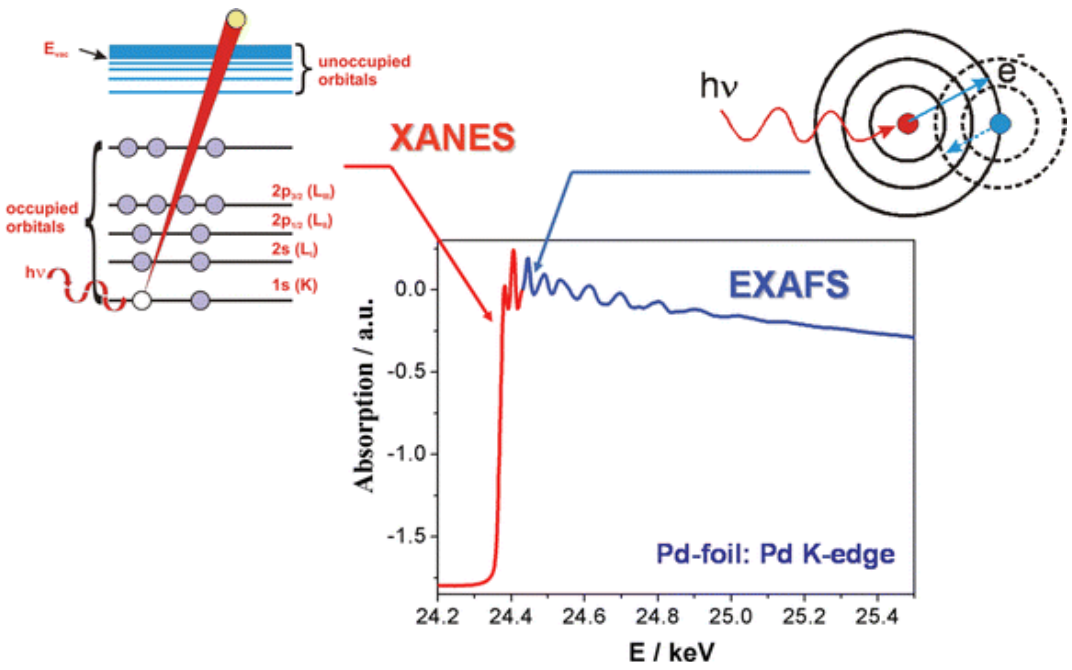

Figure 1-2. Principle of X-ray absorption near edge structure (XANES) and extended X-ray absorption fine structure (EXAFS) spectroscopy. Adapted from reference 16 with copyright permission.

XANES is the part close to the absorption edge when the energy of the absorbed incident radiation equals electron binding energy. This energy is determined by the atom involved, the quantum numbers of inner-shell electrons excited, and the electronic configuration of the valence band. Thus, XANES analysis can provide us with information on the orientation (symmetry) of unoccupied orbitals and the electron configuration (oxidation state of atom involved). For example, studies utilizing Pt L_3 edge XANES in acidic media have revealed that OH adsorption on platinum in acidic condition occurs in an atop configuration (1-fold) at low potentials, followed by 2- and 3-fold symmetries at more positive electrode potential[17].

As for EXAFS, which is caused by the interference between the emitted electrons and the electron waves backscattered by neighboring atoms, can reveal more structural information including neighboring atomic species, bond distances, and coordination numbers. By comparing K-Edge EXAFS spectra under different conditions, Jia and coworkers have found that the effect

of pH, cation, and surface transition metal on the platinum HER/HOR kinetics can be explained by the shuffling of interfacial water[18].

2.2 In situ infrared spectroscopy

Even though infrared (IR) spectroscopy is among the most popular tools for investigating the molecular structure and bonding information, its application in studying electrode/electrolyte interfaces was not successful mainly due to the fact that solvents (mostly water) strongly absorb IR radiation. This will also make the separation between bulk signal and surface signal extremely difficult, questioning the surface specificity of the technique.

The pioneering work by Bewick et al. in 1981 provides a solution to the limitations mentioned above[19]. They developed the technique called electrochemically modulated IR spectroscopy (EMIRS), as a specialized version of infrared reflection–absorption spectroscopy (IRAS, IR-RAS, also known as RAIRS)[20]. By pressing the surface very close to the infrared-transmitting window, the path length through water can be minimized. Even though the absorption bands by the thin bulk layer were still too strong and the signals from the interface were hardly discernable. This challenge was resolved by carrying the spectroscopy measurement at various potentials and making comparisons. In most situations, the bulk phase signal is less affected by the change of potential, thus the variation of spectra is mainly caused by differences in surface structure.

As a result of the development of commercial Fourier transform infrared (FTIR) spectrometers, EMIRS further evolved into SNIFTIRS (subtractively normalized interfacial Fourier transform infrared spectroscopy) with comparable signal to noise ratio and the ability to monitor the changes accompanying irreversible voltammetric reactions (**Figure 1-3a**). By

investigating the potential dependent in-situ FTIR reflection-absorption spectra of Pt(111) electrode in $HClO_4$ solution, Xia and coworkers found that water orientation changes from hydrogen down to oxygen down at around 0.35 V vs. RHE, which indicates the potential of zero charge (pzc) of platinum (111) is close to this value[10]. What's more, an increased water-platinum interaction was observed at potential higher than 0.50 V vs. RHE, which causes H_2O dissociation at the surface with the formation of adsorbed hydroxyl group.

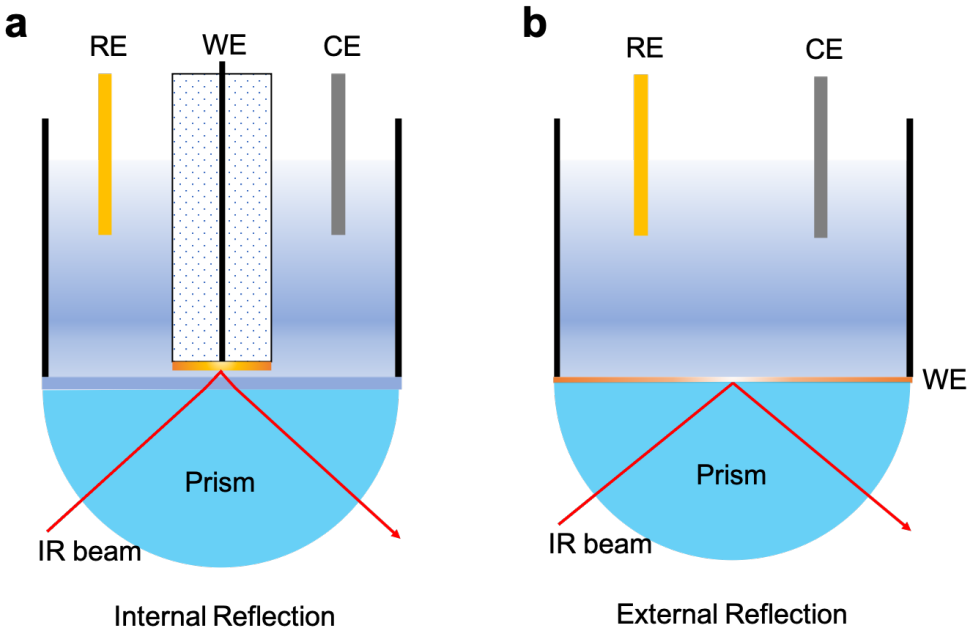

Figure 1-3. Schematic representations of in-situ FTIRS cell. (a) Internal reflection setup for IRRAS. (b)External reflection setup for ATR-IRS. RE: reference electrode; CE: counter electrode; WE: working electrode.

In situ IRAS features a very low solution thickness of 2-3 μm. This means the technique would suffer from the downside of a greatly suppressed diffusion of the reactants and products. To avoid this problem, a different setup known as internal-reflection-type attenuated total reflection IR spectroscopy (ATR-IRS) can be used. As shown in **Figure 1-3b**, instead of transmitting through the solution side, the incident IR radiation reflects on the side of the prism. By coating a thin metal layer on the side of the prism that's in contact with the solution, some of

the IR light can penetrate into the solution and interacts with the adsorbed species at the electrode/electrolyte interface. The sensitivity and surface selectivity of ATR-IRS can be further improved by controlling the property and arrangement of the coated metal thin film, which is also known as surface-enhanced IR absorption spectroscopy (SEIRAS or ATR-SEIRAS).

For metals like Au, Cu and Ag, controlling the thin film's roughness would lead to enhancement of IR absorption. Thanks to a higher sensitivity of SEIRAS compared to traditional IR reflection-absorption spectroscopy (IRRAS), Xu and coworkers investigated the potential-dependent behavior of water and related species at the Au/water interface over a wide pH range[21]. They observed peaks around 1680 cm^{-1} which increase with decreasing potential, and ascribed it to hydronium (H_3O^+) together with its associated species near the negatively-charged electrode surface. As for other metals without enhanced IR absorption, coating an extra layer of gold between the prism and the metal thin film would be the best solution. In a study completed by Shao and coworkers in 2020, ATR-SEIRAS was applied to monitor the vibrational wavenumber variation of interfacial water and adsorbed hydrogen on Pt surface in pH ranging from 1.1 to 12.9[ref.22]. They found the pH-dependent hydrogen binding energy (HBE), together with weakened interaction between interfacial water molecules and Pt surfaces at higher pH, lead to sluggish HER kinetics in basic condition. Although SEIRAS has several advantages including higher sensitivity and improved mass transfer compared to conventional IRRAS, it still has the disadvantage of not applicable to a well-defined single crystal surface.

2.3 Sum frequency generation spectroscopy

Sum frequency generation (SFG) is a nonlinear optical phenomenon. When two light beams with different energy spatially and temporally overlap at a location where centrosymmetry

is broken (e.g. solid/liquid interface), a new output beam with a frequency equals to the sum of incident beams would be generated[23]. In an SFG spectroscopy measurement, one visible laser with fixed frequency and another IR laser with varying frequency are utilized to generate the output beam, which is then separated from reflected incident lasers through the optical system. As shown in **Figure 1-4a**, when the frequency (energy) of IR laser matches the transition energy of absorbing species, the intensity of the beam generated through SFG would also be resonantly enhanced. Since the solution is a centrosymmetric environment, the signal of the SFG spectrum would only originate from the interface.

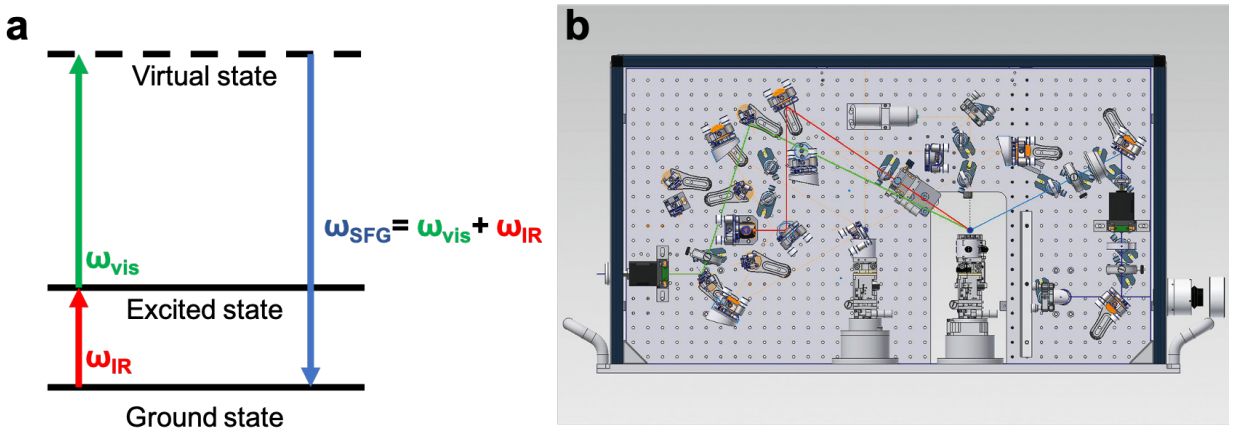

Figure 1-4. In situ sum frequency generation spectroscopy. (a) Principle of enhancement of SFG signal. (b) The structure inside an SFG spectrometer. Adapted from https://ekspla.com/product/sfg-spectrometer/.

Similar to in situ IR spectroscopy mentioned in the previous part, both internal- and external- reflection configuration can be used when performing SFG spectroscopy in electrode/electrolyte interface study. The latter is more favored due to less IR beam absorption by the solution. In a recent study of gold/water interface by SFG spectroscopy, a potential-dependent SFG intensity was observed[24]. The authors ascribe this observation to the variation of water molecule's orientation and density at the interface caused by surface potential. While similar in

many aspects, SFG spectroscopy requires more complicated apparatus (especially optical equipment) compared to in situ IR spectroscopy, which is one major downside of this technique.

2.4 In situ surface enhanced Raman spectroscopy

When a sample is illuminated by incident light with a certain frequency, most photons are elastically scattered (Rayleigh scattering) while a tiny fraction of photons is inelastically scattered. Raman spectroscopy relies upon the inelastic scattering of photons, known as Raman scattering. The information gathered through Raman spectroscopy is essentially same as IR spectroscopy: vibrational modes in the system. The difference in selection rules for these two methods makes them complementary to each other. What's more, while IR spectroscopy is recording the absorption of light with certain energy, Raman spectroscopy is monitoring the energy difference between incident light and inelastically scattered light (**Figure 1-5**).

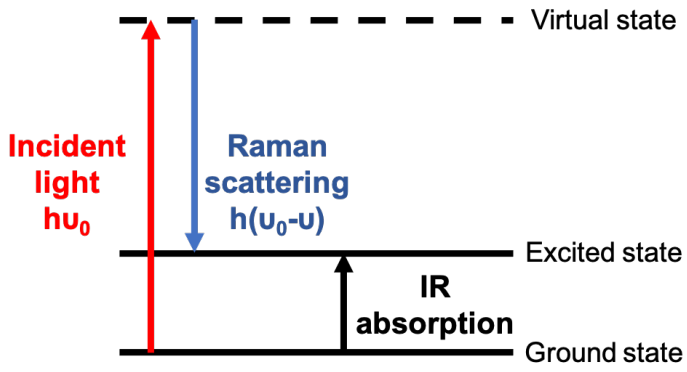

Figure 1-5. Energy-level diagram showing the difference between IR spectra and Raman spectra.

Though observed as early as 1928, Raman scattering was not widely applied for surface investigation until the discovery of Raman intensity enhancement on a roughened surface[25]. The technique developed was known as surface enhanced Raman spectroscopy (SERS). Compared to IR spectroscopy, SERS is more surface sensitive and not limited to a thin solution layer configuration. However, it has similar drawbacks as SEIRAS: only a very limited range of

materials can be used and single crystal surfaces cannot be analyzed. To extend the range of materials available for SERS, two different approaches were explored over the past 20 years and both were proven to be successful.

One solution is depositing Raman active nanostructures on top of the target surface. It was found that Raman intensity would be enhanced by a factor of approximately 10^6 when gold nanoparticles are deposited on top of a metal surface[26]. More importantly, the metal substrate below could be a single crystal surface with non-SERS-active material. Based on the configuration, the authors named the technique gap-mode Raman spectroscopy. Later on, Tian's Group further developed this method into shell-isolated nanoparticle-enhanced Raman spectroscopy (SHINERS) by coating a layer of inert silica shell over the gold nanoparticles to prevent aggregation and to separate them from direct contact with the probed material[14, 27-29]. With Raman signal enhancement near the surface of different platinum crystal planes, direct spectroscopic evidence for ORR intermediates was acquired[28]. They found that for ORR in acidic condition, the reaction pathway on platinum occurs through the formation of HO_2* or OH*; regarding basic condition, deprotonation causes the O_2^- species to be the intermediate.

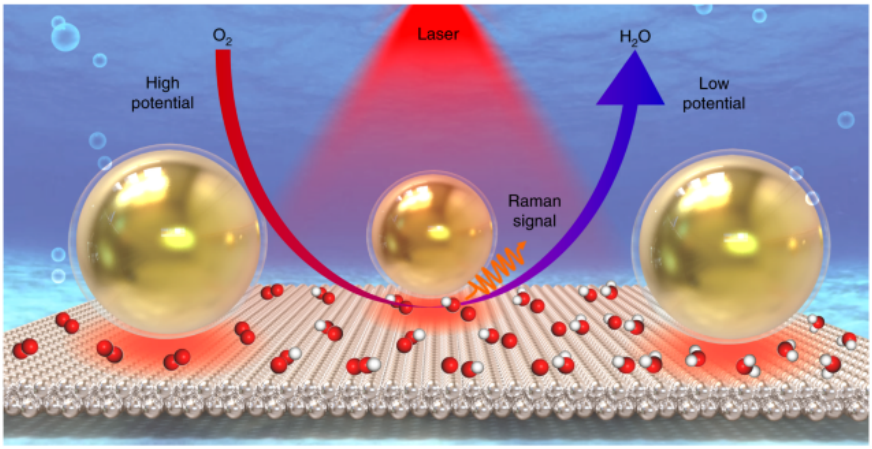

Figure 1-6. Schematic representation of shell-isolated nanoparticle-enhanced Raman spectroscopy (SHINERS). Adapted from reference 28 with copyright permission.

Another solution is the strategy of 'borrowing the SERS activity' by coating the desired material on highly SERS-active Au nanoparticles[30-32]. This strategy is suitable for material that requires a specific crystal phase/particle size to exhibit high catalytic activity. For example, molybdenum disulfide (MoS_2), as a classical example of transition metal dichalcogenide (TMD), has emerged as a favorable cost-effective catalyst for hydrogen evolution reaction. However, the mechanism and active sites of HER on MoS_2 are still poorly understood because it has limited SERS activity. By successfully synthesizing Ag@MoS_2 core-shell heterostructure with SERS enhancement ability, Zhang and coworkers investigated the bonding information during the HER process of MoS_2 and discovered that sulfur atom serves as the active site where S-H bond with vibrational wavenumber of 2532 cm^{-1} is formed[33].

2.5 Electrochemical quartz crystal microbalance (EQCM) technique

As a combination of an electrochemical cell and quartz crystal microbalance, EQCM (also known as EQCN: electrochemical quartz crystal nanobalance) is a highly sensitive in-situ measurement. As shown in **Figure 1-7a**, two electrodes are attached on both sides of the quartz crystal to generate standing waves with a certain resonant frequency by applying an alternating electric field[34]. What's more, one of the electrodes will contact the solution and serve as working electrode (WE) in the three-electrode system. When a layer of material or molecule is deposited/adsorbed onto the surface of the working electrode, the fundamental frequency will change depending on the mass variation. By correlating the change in surface mass (Δm) and charge (Δq by CV current integration), the average molecular weight of adsorbed species can be determined[35-37].

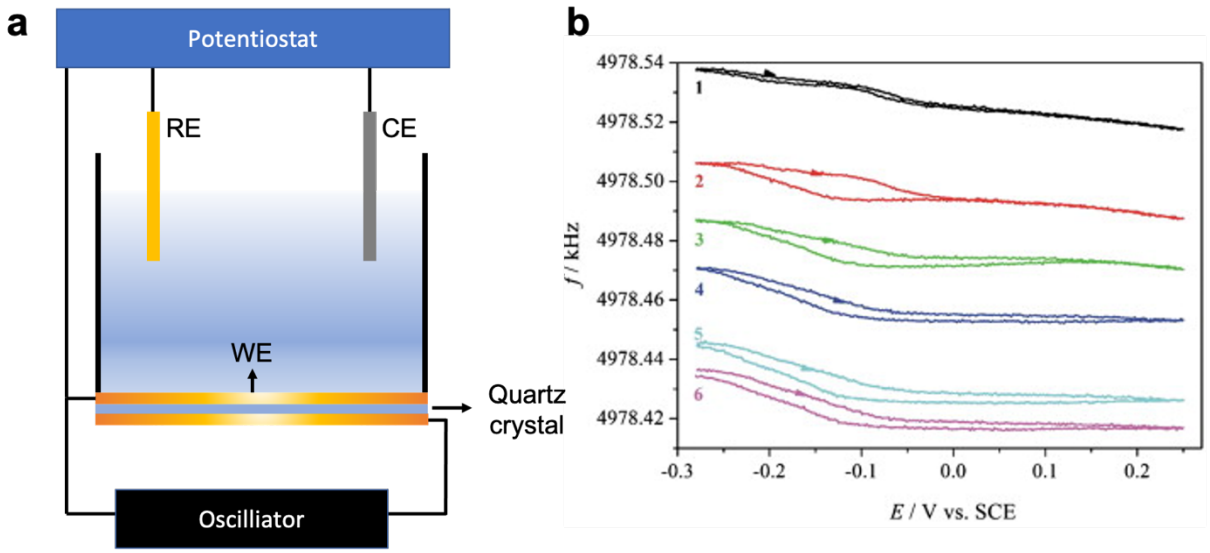

Figure 1-7. Schematic representations and result of Cs^+ adsorption of EQCM. (a) Typical setup for EQCM. RE: reference electrode; CE: counter electrode; WE: working electrode. (b) EQCM response of a platinum electrode in contact with (1) 0.0 (2) 0.029, (3) 0.056, (4) 0.1, (5) 0.12, (6) 0.136 mol/L of Cs_2SO_4. Adapted from reference 38, with copyright permission.

As shown in **Figure 1-7b**, the effect of Cs^+ towards the under-potential deposition of hydrogen (H_{upd}) is investigated with EQCM[38]. The mass change at low potential region is much higher when Cs^+ is introduced in the system, which can be explained by the co-adsorption of Cs^+ with hydrogen atoms. Though EQCM is one of the most surface selective characterization methods, it is not applicable to complicated electrochemical processes because the mass change observed may be interpreted in different molecular combinations.

3. Electrical transport spectroscopy (ETS)

The classic picture of an electrochemical interface involves molecules, intermediates, solid electrode surface, and the surrounding electrolyte double layer. Such complexity often interferes with any form of radiation signals from a specific target (e.g., FTIR signals from surface adsorbed chemical species), posing a considerable technical challenge in the application of conventional spectroscopic strategies for electrochemical characterizations. As introduced in the previous part, various techniques were newly developed to achieve in situ monitor of the catalytic interface during an electrochemical process, which is considered most informative yet extremely challenging. However, these approaches have their limitation such as unusual device design or limited material type. What's more, ensuring the surface selectivity of signals detected is always the biggest challenge of any characterization. To address this issue, our group has specifically developed an in situ characterization method, known as Electrical transport spectroscopy (ETS), for probing electrochemical interfaces[39]. The following sections will give a detailed introduction of the underlying principle and experimental setup of ETS.

3.1 Underlying principle of ETS: electron scattering effect at the metal surface

The theory basis of ETS is diffusive scattering caused by the molecules adsorbed on a metallic surface[40-42]. At room temperature, electrons in the metal are scattered by the lattice vibrations in metals (phonons), other electrons, impurities, and other defects (grain boundary)[43]. As a result, the electrons would have a limited mean free path (λ). The specularity coefficient, p, describes the portion of electrons specularly scattered at the metal surface. The remaining fraction (1-p) of the scattered electrons would be diffusively scattered. Based on the model developed by

Fuchs and Sondheimer[40], resistance change of one-dimensional cylindrical wires can be described by the following equations:

$$\rho = \rho_0 \left(1 + \frac{3}{4}(1-p)\frac{\lambda}{d}\right) \quad (d \gg \lambda)$$

$$\rho = \rho_0 \left(\frac{1-p}{1+p} \times \frac{\lambda}{d}\right) \quad (d \ll \lambda)$$

where ρ_0 is the resistivity of bulk metal, ρ is the resistivity of metallic wire and d is the wire diameter. Molecules and ions adsorbed on the metal surface can act as diffusive scattering centers which lead to a higher fraction (smaller p) of electrons to be diffusively scattered. As shown in both equations, when the dimension of a metallic structure gets close to the mean free path of the electron within it, the diffusive scattering (surface scattering) induced by substances at the surface can produce a significant change in resistivity.

This phenomenon lays the foundation of the method's reliability in studying the trivial effects on solid/liquid interface caused by the adsorption of different species in the electrolyte. Since each adsorbate exhibits distinct effective scattering cross-section, the change of conductivity would be different. During an electrochemical cycle, various substances are adsorbed onto the surface of catalyst, the change of conductivity of the catalytic nanostructure can serve as a signaling pathway to the current status of the interface between catalyst and solution.

3.2 Experimental setup of ETS

With a proper design of device structure based on metallic nanowires and electronic measurement configuration, we can carry out electrical transport measurement of the metallic nanowires in situ while in-device cyclic voltammetry is conducted at the same time. Our studies adopt an electrical measurement configuration based on a modified electrolyte-gated transistor measurement method, instead of using the electrolyte gating only to induce an electrical double-

layer on the nanowire surface, a three-electrode system was adopted and the gate voltage was extended to a range so that the desired electrochemical reactions could occur (as illustrated in **Figure 1-8**).

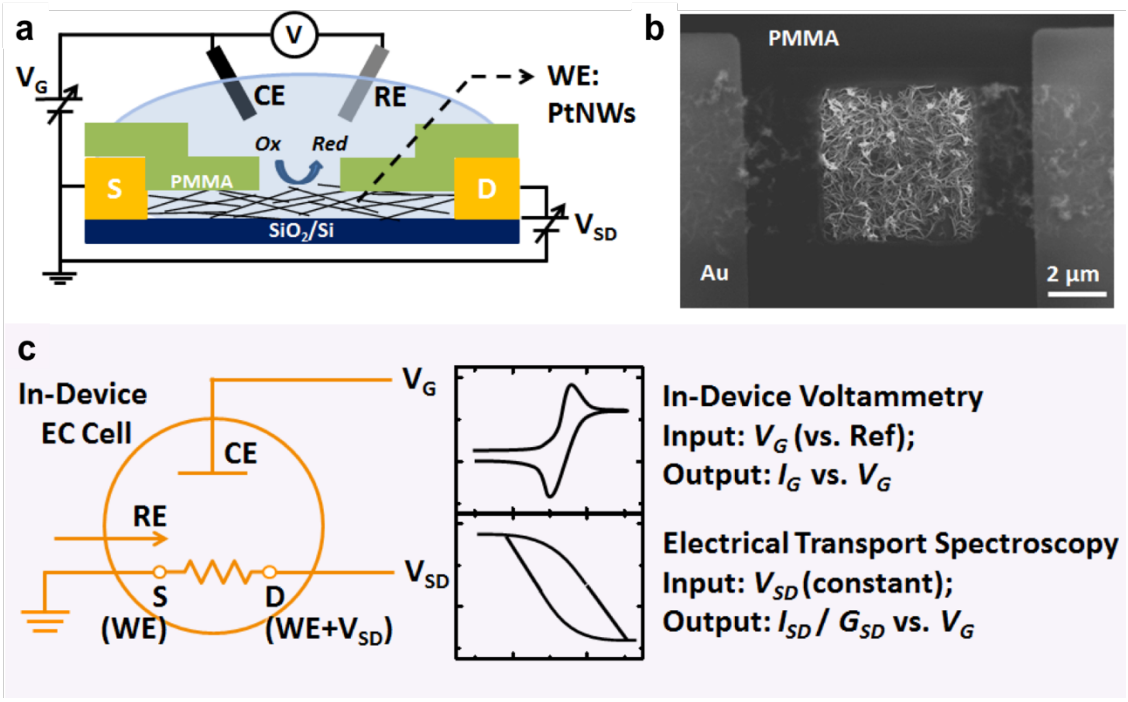

Figure 1-8. Device structure and working principle of in situ electrical transport spectroscopy (ETS) measurement simultaneously with cyclic voltammetry. (a) Schematic illustration of the platinum nanowires (PtNWs) device with electrochemical cell on it. (b) SEM image of a device cell showing polymethyl methacrylate (PMMA) covered the gold electrodes and the exposed PtNWs network in the PMMA window. (c) Schematic diagram of in-device voltammetry and ETS for in situ monitoring of the electrochemical interfaces. CE, counter electrode; RE, reference electrode; WE, working electrode; S, Source; D, Drain. Adapted from citation 39, with copyright permission.

The detailed process of device fabrication and experimental condition will be expanded in each following chapter. In short, ultrafine PtNWs were prepared through wet chemistry[44], assembled into a thin film using co-solvent evaporation, and deposited onto Si/SiO_2 wafer with pre-patterned gold electrodes. A layer of electrochemically inert polymethyl methacrylate (PMMA) was then employed to isolate the electrode (with an electrochemical window defined by electron-

beam lithography) and ensuring airtightness of the microfluidic system. Compared to an open chambered configuration, a microfluidic system was introduced to improve solution exchange efficiency. A DC source-measure-unit (SMU, Agilent 2902a) was used to apply gate voltage (V_G) and collecting Faradic current (electrochemical response), while the conductance change of the device is recorded. Compared to the preliminary version of ETS, specific improvements were made to secure device stability and achieve the target of a certain project, which will be explained separately.

3.3 In situ ETS result of PtNWs in acidic condition

The results from our preliminary study show that electrical transport properties of ultrafine platinum nanowires (PtNWs) are highly sensitive to electrochemical surface state, and can be used as an effective signaling pathway for in situ probing the electrochemical interfaces[39]. A typical in-device CV and in situ electrical transport signal of a PtNW device is shown in **Figure 1-9a**. The I_G-V_G relationship (black curve in **Figure 1-9a**) closely resembles the typical CV characteristics of polycrystalline Pt surface[45], containing five redox regions: hydrogen evolution reaction (HER); H adsorption/desorption region (H_{upd}); double layer (D.L.) region; surface oxide formation/ reduction region (O_{upd}) and oxygen evolution reaction (OER). This result demonstrates the validity of the in-device CV measurement.

The red curve in **Figure 1-9a** shows the conductance characteristics of PtNWs (normalized conductance change: $\Delta G_{SD}/G_{SD}$) under different gate voltage that is monitored simultaneously with the CV measurement. The curve of conductance change in **Figure 1-9a** can be divided into three sections :

(1) At relatively negative potential, adsorption/desorption of hydrogen on platinum surface results in an obvious change in conductance, as indicated by the yellow box in **Figure 1-9a**. The device exhibits the highest conductivity in this region, which can be attributed to a weaker diffusive scattering of electrons by hydrogen atom compared to water and other adsorbates. A similar phenomenon was observed before when H_2 gas adsorbed onto platinum nanowire[41].

(2) The conductance change is relatively small in the double layer region, where the surface of PtNWs is predominantly occupied by a layer of adsorbed water molecules. Even though charge will affect the conductivity of a metal thin film[46-48], the relative change observed is usually less than 1% due to a relatively high carrier density in metal.

(3) In the positive potential region, corresponding to the formation/reduction of surface oxygenated species (also shown in CV curve), a more pronounced conductance change (purple box in **Figure 1-9a**) can be observed together with an obvious hysteresis. In the positive-going scan, the conductance value decreases gradually at the beginning, which is followed by a much steeper drop. The gradual decrease can be ascribed to the adsorption of hydroxyl species (OH_{ads}), while the steep drop is associated with the formation of surface oxide (PtO_x). Compared to a hydrogen atom and water molecule, the strongly bonded oxygen atom has a greater scattering cross-section, which resulted in the obvious drop of device conductivity. Besides, the formation of platinum oxide further reduces the free electron density in the nanowire. In the negative-going scan, the device conductance is relatively stable until the onset potential of the oxide reduction, which is also shown by a cathodic peak in the CV curve.

Moreover, a differentiation of the normalized conductance change (**Figure 1-9b**) can be further conducted to produce electrical transport spectroscopy (dETS) for a more convenient and efficient visualization and analysis of the electrical transport characteristics. **Figure 1-9c** gives a

series of qualitative illustrations summarizing the correlation between electronic signals of the device and the electrochemical surface state of the material.

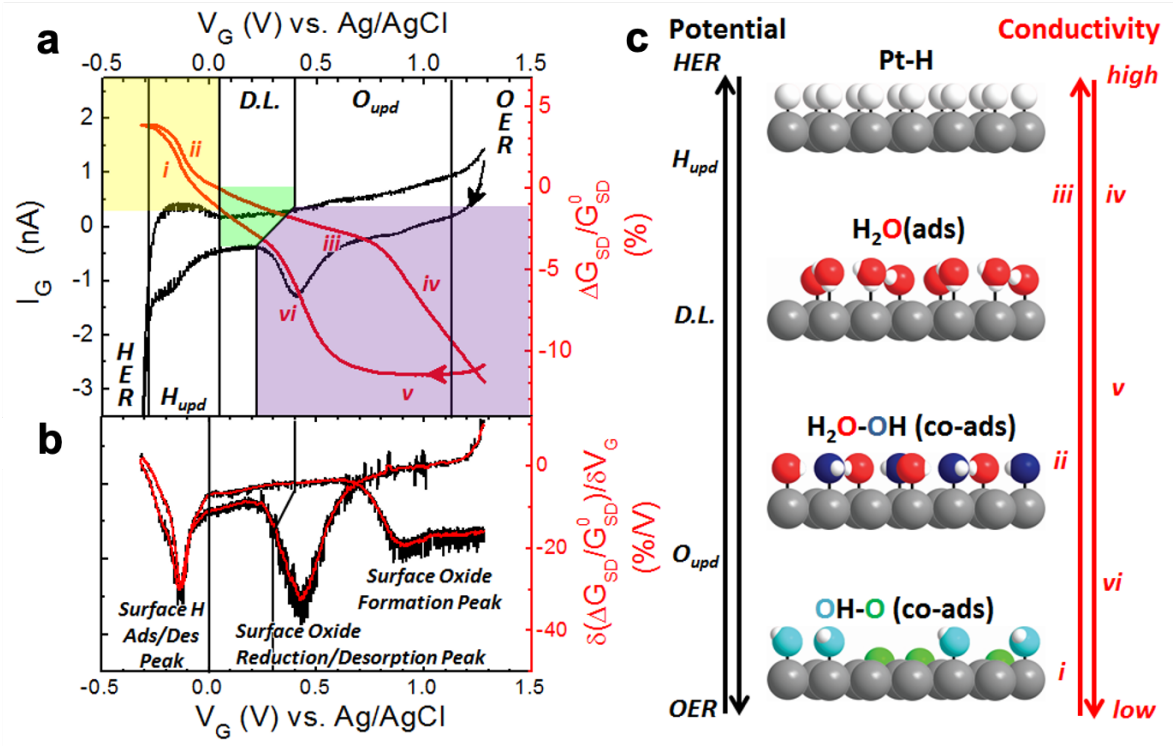

Figure 1-9. In situ ETS monitoring of Pt surface chemistry during electrochemical process. (a) I_G-V_G (black curve) and normalized conductance change $\Delta G_{SD}/G_{SD}$-V_G (red curve) characteristics of a typical PtNW device. I_G-V_G resembles the typical CV characteristics of a polycrystalline Pt surface, containing redox regions of certain electrochemical processes. $\Delta G_{SD}/G_{SD}$-V_G curve can also be divided into three regions correspondingly, which are marked with blue, green and red boxes. (b) Electrical spectroscopic data resulted from differentiated analysis of $\Delta G_{SD}/G_{SD}$ -V_G result, showing spectral peak characteristics. (c) Schematic illustrations of different Pt surface conditions with the sweeping electrochemical potentials (left black axis) and the corresponding conductivity changes (right red axis, labels shown along the axis are corresponding to the labels shown on G_{SD} curve in a). Pt atoms are grey, H atoms are white, O atoms are red in H_2O_{ads}, blue in OH_{ads}, and green in O_{ads} for a visual guide to the different scattering effects. Adapted from citation 39, with copyright permission.

The result acquired will assist us in understanding the relationship between the electrochemical interface (encompassing catalyst surface and electrolyte double layer structure)

and key physical/chemical interactions (adsorption, bonding reformation, desorption, etc.). This fundamental understanding can be used to guide the design of novel nanostructures with improved electrocatalytic properties. The platinum nanowires device serves as an electronic probe, alternative to the existing spectroscopic probes, for in situ monitoring the dynamic electrochemical interface between the metallic nanostructures and the electrolyte under different electrochemical conditions. Such electrochemical interfaces are difficult to access by the radiation but can be easily probed by electrical current flowing through the ultrafine metallic nanostructures that are highly sensitive to the surface scattering effect of the adsorbed chemical species.

With this novel nanoelectronic measurement approach, we are able to conduct a series of systematic investigations of nano-electrocatalysts surface chemistry for a wide range of fundamentally or practically important electrocatalytic reactions. First, we investigated competitive anionic chemisorption on the platinum surface and its' relationship with ORR kinetics (**Chapter 2**). After that, we acquired ETS results in a serials of pH conditions and discovered the pKa of hydronium adsorbed on the platinum surface (**Chapter 3**). At last, we explored the ETS configuration's potential in sensing hydrogen peroxide and DNA molecules (**Chapter 4**).

4. Reference

1. Seh, Z. W.; Kibsgaard, J.; Dickens, C. F.; Chorkendorff, I.; Nørskov, J. K.; Jaramillo, T. F., Combining theory and experiment in electrocatalysis: Insights into materials design. *Science* **2017,** *355* (6321).

2. Guo, S.; Wang, E., *Noble metal nanomaterials: Controllable synthesis and application in fuel cells and analytical sensors*. 2011; Vol. 6, p 240-264.

3. Cheng, F.; Chen, J., Metal-air batteries: from oxygen reduction electrochemistry to cathode catalysts. *Chemical Society Reviews* **2012,** *41* (6), 2172-2192.

4. Chen, A.; Holt-Hindle, P., Platinum-Based Nanostructured Materials: Synthesis, Properties, and Applications. *Chemical Reviews* **2010,** *110* (6), 3767-3804.

5. Rossmeisl, J.; Qu, Z. W.; Zhu, H.; Kroes, G. J.; Nørskov, J. K., Electrolysis of water on oxide surfaces. *Journal of Electroanalytical Chemistry* **2007,** *607* (1-2), 83-89.

6. Dubouis, N.; Grimaud, A., The hydrogen evolution reaction: from material to interfacial descriptors. *Chemical Science* **2019,** *10* (40), 9165-9181.

7. Ledezma-Yanez, I.; Wallace, W. D. Z.; Sebastián-Pascual, P.; Climent, V.; Feliu, J. M.; Koper, M. T. M., Interfacial water reorganization as a pH-dependent descriptor of the hydrogen evolution rate on platinum electrodes. *Nature Energy* **2017,** *2* (4), 17031.

8. Velasco-Velez, J.-J.; Wu, C. H.; Pascal, T. A.; Wan, L. F.; Guo, J.; Prendergast, D.; Salmeron, M., The structure of interfacial water on gold electrodes studied by x-ray absorption spectroscopy. *Science* **2014,** *346* (6211), 831-834.

9. Toney, M. F.; Howard, J. N.; Richer, J.; Borges, G. L.; Gordon, J. G.; Melroy, O. R.; Wiesler, D. G.; Yee, D.; Sorensen, L. B., Voltage-dependent ordering of water molecules at an electrode–electrolyte interface. *Nature* **1994,** *368* (6470), 444-446.

10. Iwasita, T.; Xia, X., Adsorption of water at Pt(111) electrode in HClO4 solutions. The potential of zero charge. *Journal of Electroanalytical Chemistry* **1996,** *411* (1), 95-102.

11. Ataka, K.-i.; Yotsuyanagi, T.; Osawa, M., Potential-Dependent Reorientation of Water Molecules at an Electrode/Electrolyte Interface Studied by Surface-Enhanced Infrared Absorption Spectroscopy. *The Journal of Physical Chemistry* **1996,** *100* (25), 10664-10672.

12. Zhang, Y.-J.; Su, Z.-F.; Li, J.-F.; Lipkowski, J., What Vibrational Spectroscopy Tells about Water Structure at the Electrified Palladium–Water Interface. *The Journal of Physical Chemistry C* **2020,** *124* (24), 13240-13248.

13. Gardner, A. M.; Saeed, K. H.; Cowan, A. J., Vibrational sum-frequency generation spectroscopy of electrode surfaces: studying the mechanisms of sustainable fuel generation and utilisation. *Physical Chemistry Chemical Physics* **2019,** *21* (23), 12067-12086.

14. Li, C.-Y.; Le, J.-B.; Wang, Y.-H.; Chen, S.; Yang, Z.-L.; Li, J.-F.; Cheng, J.; Tian, Z.-Q., In situ probing electrified interfacial water structures at atomically flat surfaces. *Nature Materials* **2019,** *18* (7), 697-701.

15. Toney, M.; Melendres, C.; Tadjeddine, A., Synchrotron Techniques in Interfacial Electrochemistry. *Kluwer Academic Publishers, Netherlands* **1994**, 109-125.

16. Grunwaldt, J.-D.; Baiker, A., In situ spectroscopic investigation of heterogeneous catalysts and reaction media at high pressure. *Physical Chemistry Chemical Physics* **2005,** *7* (20), 3526-3539.

17. Teliska, M.; O'Grady, W.; Ramaker, D., Determination of O and OH adsorption sites and coverage in situ on Pt electrodes from Pt L23 X-ray absorption spectroscopy. *The Journal of Physical Chemistry B* **2005,** *109* (16), 8076-8084.

18. Liu, E.; Jiao, L.; Li, J.; Stracensky, T.; Sun, Q.; Mukerjee, S.; Jia, Q., Interfacial water shuffling the intermediates of hydrogen oxidation and evolution reactions in aqueous media. *Energy & Environmental Science* **2020,** *13* (9), 3064-3074.

19. Bewick, A.; Kunimatsu, K.; Robinson, J.; Russell, J. W., IR vibrational spectroscopy of species in the electrode-electrolyte solution interphase. *Journal of Electroanalytical Chemistry and Interfacial Electrochemistry* **1981,** *119* (1), 175-185.

20. Hollins, P., Infrared reflection–absorption spectroscopy. *Encyclopedia of Analytical Chemistry: Applications, Theory and Instrumentation* **2006**.

21. Dunwell, M.; Yan, Y.; Xu, B., A surface-enhanced infrared absorption spectroscopic study of pH dependent water adsorption on Au. *Surface Science* **2016,** *650*, 51-56.

22. Zhu, S.; Qin, X.; Yao, Y.; Shao, M., pH-Dependent Hydrogen and Water Binding Energies on Platinum Surfaces as Directly Probed through Surface-Enhanced Infrared Absorption Spectroscopy. *Journal of the American Chemical Society* **2020,** *142* (19), 8748-8754.

23. Shen, Y., Surfaces probed by nonlinear optics. *Surface Science* **1994,** *299*, 551-562.

24. Tong, Y.; Lapointe, F.; Thämer, M.; Wolf, M.; Campen, R. K., Hydrophobic water probed experimentally at the gold electrode/aqueous interface. *Angewandte Chemie International Edition* **2017,** *56* (15), 4211-4214.

25. Fleischmann, M.; Hendra, P. J.; McQuillan, A. J., Raman spectra of pyridine adsorbed at a silver electrode. *Chemical physics letters* **1974,** *26* (2), 163-166.

26. Ikeda, K.; Sato, J.; Fujimoto, N.; Hayazawa, N.; Kawata, S.; Uosaki, K., Plasmonic enhancement of Raman scattering on non-SERS-active platinum substrates. *The Journal of Physical Chemistry C* **2009,** *113* (27), 11816-11821.

27. Li, J. F.; Huang, Y. F.; Ding, Y.; Yang, Z. L.; Li, S. B.; Zhou, X. S.; Fan, F. R.; Zhang, W.; Zhou, Z. Y.; Ren, B., Shell-isolated nanoparticle-enhanced Raman spectroscopy. *nature* **2010,** *464* (7287), 392-395.

28. Dong, J.-C.; Zhang, X.-G.; Briega-Martos, V.; Jin, X.; Yang, J.; Chen, S.; Yang, Z.-L.; Wu, D.-Y.; Feliu, J. M.; Williams, C. T.; Tian, Z.-Q.; Li, J.-F., In situ Raman spectroscopic evidence for oxygen reduction reaction intermediates at platinum single-crystal surfaces. *Nature Energy* **2019,** *4* (1), 60-67.

29. Li, J. F.; Tian, X. D.; Li, S. B.; Anema, J. R.; Yang, Z. L.; Ding, Y.; Wu, Y. F.; Zeng, Y. M.; Chen, Q. Z.; Ren, B., Surface analysis using shell-isolated nanoparticle-enhanced Raman spectroscopy. *Nature protocols* **2013,** *8* (1), 52-65.

30. Park, S.; Yang, P.; Corredor, P.; Weaver, M. J., Transition metal-coated nanoparticle films: vibrational characterization with surface-enhanced Raman scattering. *Journal of the American Chemical Society* **2002,** *124* (11), 2428-2429.

31. Tian, Z.-Q.; Yang, Z.-L.; Ren, B.; Li, J.-F.; Zhang, Y.; Lin, X.-F.; Hu, J.-W.; Wu, D.-Y., Surface-enhanced Raman scattering from transition metals with special surface morphology and nanoparticle shape. *Faraday discussions* **2006,** *132*, 159-170.

32. Jiang, Y.-X.; Li, J.-F.; Wu, D.-Y.; Yang, Z.-L.; Ren, B.; Hu, J.-W.; Chow, Y. L.; Tian, Z.-Q., Characterization of surface water on Au core Pt-group metal shell nanoparticles coated electrodes by surface-enhanced Raman spectroscopy. *Chemical communications* **2007,** (44), 4608-4610.

33. Chen, J.; Liu, G.; Zhu, Y.-z.; Su, M.; Yin, P.; Wu, X.-j.; Lu, Q.; Tan, C.; Zhao, M.; Liu, Z., Ag@ MoS2 core–shell heterostructure as SERS platform to reveal the hydrogen

evolution active sites of single-layer MoS2. *Journal of the American Chemical Society* **2020,** *142* (15), 7161-7167.

34. Buttry, D. A.; Ward, M. D., Measurement of interfacial processes at electrode surfaces with the electrochemical quartz crystal microbalance. *Chemical Reviews* **1992,** *92* (6), 1355-1379.

35. Inzelt, G.; Berkes, B. B.; Kriston, Á., Electrochemical nanogravimetric studies of adsorption, deposition, and dissolution processes occurring at platinum electrodes in acid media. *Pure and Applied Chemistry* **2010,** *83* (2), 269-279.

36. Shimazu, K.; Kita, H., In situ measurements of water adsorption on a platinum electrode by an electrochemical quartz crystal microbalance. *Journal of Electroanalytical Chemistry* **1992,** *341* (1-2), 361-367.

37. Inzelt, G.; Berkes, B. B.; Kriston, Á.; Székely, A., Electrochemical nanogravimetric studies of platinum in acid media. *Journal of Solid State Electrochemistry* **2011,** *15* (5), 901-915.

38. Berkes, B.; Székely, A.; Inzelt, G., Effect of Cs+ ions on the electrochemical nanogravimetric response of platinum electrode in acid media. *Electrochemistry communications* **2010,** *12* (8), 1095-1098.

39. Ding, M.; He, Q.; Wang, G.; Cheng, H.-C.; Huang, Y.; Duan, X., An on-chip electrical transport spectroscopy approach for in situ monitoring electrochemical interfaces. *Nature Communications* **2015,** *6*, 7867.

40. Sondheimer, E. H., The mean free path of electrons in metals. *Advances in Physics* **2001,** *50* (6), 499-537.

41. Yang, F.; Donavan, K. C.; Kung, S.-C.; Penner, R. M., The Surface Scattering-Based Detection of Hydrogen in Air Using a Platinum Nanowire. *Nano Letters* **2012,** *12* (6), 2924-2930.

42. Wissmann, P.; Müller, K., *Surface physics*. Springer: 2006; Vol. 77.

43. Coffey, K., Electron scattering in metallic thin films. In *Metallic Films for Electronic, Optical and Magnetic Applications*, Elsevier: 2014; pp 422-453.

44. Xia, B. Y.; Wu, H. B.; Yan, Y.; Lou, X. W.; Wang, X., Ultrathin and Ultralong Single-Crystal Platinum Nanowire Assemblies with Highly Stable Electrocatalytic Activity. *Journal of the American Chemical Society* **2013,** *135* (25), 9480-9485.

45. Climent, V.; Feliu, J. M., *Thirty years of platinum single crystal electrochemistry*. 2011; Vol. 15, p 1297-1315.

46. Fujihara, M.; Kuwana, T., Studies of electrochemical interfaces of thin PT film electrodes by surface conductance. *Electrochimica Acta* **1975,** *20* (8), 565-573.

47. Tucceri, R., A review about the surface resistance technique in electrochemistry. *Surface Science Reports* **2004,** *56* (3), 85-157.

48. Rath, D. L., Studies of electrode resistance in the electrochemical cell. *Journal of Electroanalytical Chemistry and Interfacial Electrochemistry* **1983,** *150* (1-2), 521-534.

Chapter 2. Electrical transport spectroscopy (ETS) supported in situ monitoring of competitive interfacial anionic chemisorption on platinum surface

1. Introduction and background

The development of future sustainable energy technologies relies critically on our understanding of electrocatalytic reactions occurring at the electrode−electrolyte interfaces, and the identification of key reaction promoters and inhibitors. Oxygen reduction reaction (ORR) based on platinum and other transition metal catalysts is crucial to the process involved in fuel cells and batteries[1, 2]. Modification of electrocatalysts in size, shape and composition (electronic structure) has led to a huge improvement of their ORR activity. Nevertheless, the difference between laboratory conditions (e.g. a controlled environment in rotating disk electrode measurements) and practical energy devices has made it challenging for the new catalysts to exhibit consistent performance. In a less controlled environment, various interfacial adsorptions may happen which could severely hinder specific reactions or even result in catalyst degradation (**Figure 2-1**).

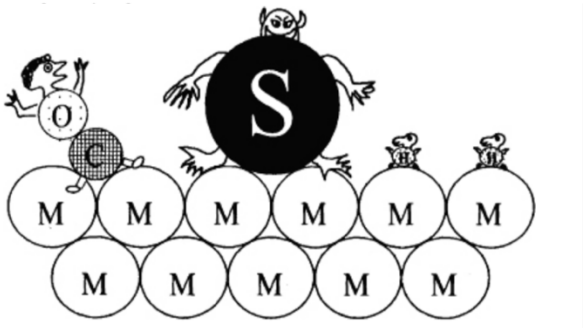

Figure 2-1. Cartoon of poisoning effect towards metal catalysts caused by sulfur and carbon monoxide. Adapted from reference 3 with copyright permission.

Hence, a better understanding of electrode/electrolyte interface under a more complex environment is vital for optimizing a specific electrochemical reaction. Though there exist utmost technical challenges, in situ investigations are always favored because they can extract information

from the interface while the active reaction is happening. As introduced in the previous chapter, the electrical transport spectroscopy (ETS) developed by our group can serve as a suitable on-chip signaling technique for in situ studies of electrode/electrolyte interface.

Here in this chapter, we present a systematic investigation of different anionic adsorption on platinum catalyst surface based on ETS[4]. Anions in a practical device may originate from the electrolyte itself or contaminants in other components, and they usually bind to the catalyst surface strongly. This competitive adsorption, also known as the poisoning effect, is highly possible to block the desired adsorption of electroactive reactants and prevent their transition into crucial reaction intermediates. Thus, an in-depth understanding of the relationship between anionic adsorption and electrochemical reaction (e.g. ORR, HER) is highly favorable. Previous investigations of anionic adsorption will be introduced separately in the following sections.

By investigating the distinct anionic adsorption feature of sulfate and halide anion with the assistance of ETS, we can derive not only qualitative but also quantitative information from the surface in a complicated electrochemical environment. What's more, we also investigated the competitive adsorption between perchlorate (ClO_4^-) and chloride anion. Our findings provide a potential solution to mitigate the undesired anionic poisoning by altering the electrolyte's composition. Further test with rotating disk electrode (RDE) has proved that the competitive anionic adsorption model may serve as a descriptor for oxygen reduction reaction on platinum catalyst.

2. Materials and methods

2.1 Synthesis of platinum nanowires (PtNWs) and preparation of PtNWs thin film

PtNWs were prepared based on a previous study[5] with slight modification. 0.6 gram of KOH was dissolved in ethylene glycol (4 mL), then mixed with 6 mL of dimethylformamide (DMF). 0.1mL of aqueous solution of K_2PtCl_6 (8 wt%) was then added and stirred for 20 min which resulted in a uniform yellow solution. The reaction mixture was transferred into a Teflon-lined autoclave, which was maintained at 150 °C for 15 h and then cooled to room temperature. The mixture was then centrifuged to collect the black powders, which were washed with ethanol and DI water repeatedly several times before the preparation of PtNWs thin film. A TEM image of platinum nanowires prepared is shown in **Figure 2-2**.

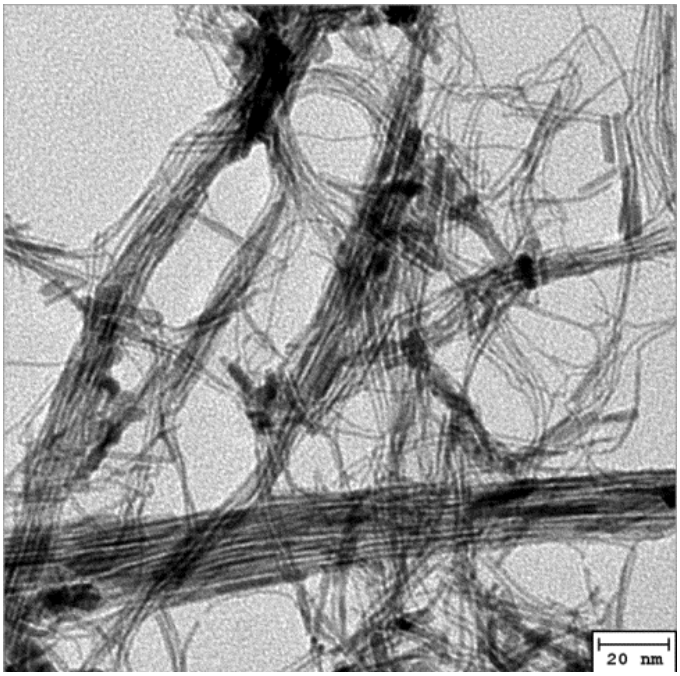

Figure 2-2. Representative TEM image of as-prepared PtNWs, bundles of nanowires can be observed. Adapted from reference 4 with copyright permission.

A free-standing film was assembled from PtNWs suspension through the co-solvent evaporation method. Typically, 800 μL of PtNWs suspensions in ethanol (0.4 mg/mL) was mixed with 1200 μL of miliQ water and 500 μL of n-Butanol. The mixture was sonicated and added drop

by drop into a beaker (about 9 cm in diameter) filled with DI water. A film of PtNWs was then formed on the water surface which would be transferred onto the device later.

2.2 Fabrication of the PtNWs device

PtNWs device is fabricated based on our previous publications[6, 7] with slight modification (**Figure 2-3**). In short, a layer of poly(methyl methacrylate) (PMMA, A8, MicroChem Corp.) was prepared by spin-coating on the substrate (p++ silicon wafer with 300 nm thermal oxide) surface with pre-patterned Au electrodes (Ti/Au, 50nm/50nm). Desired patterns were created by E-beam lithography, followed by deposition of a pre-prepared free-standing film of PtNWs through co-solvent evaporation. In order to achieve a well-controlled deposit into the desired area, the PMMA substrate was made hydrophilic by oxygen plasma treatment before the deposition.

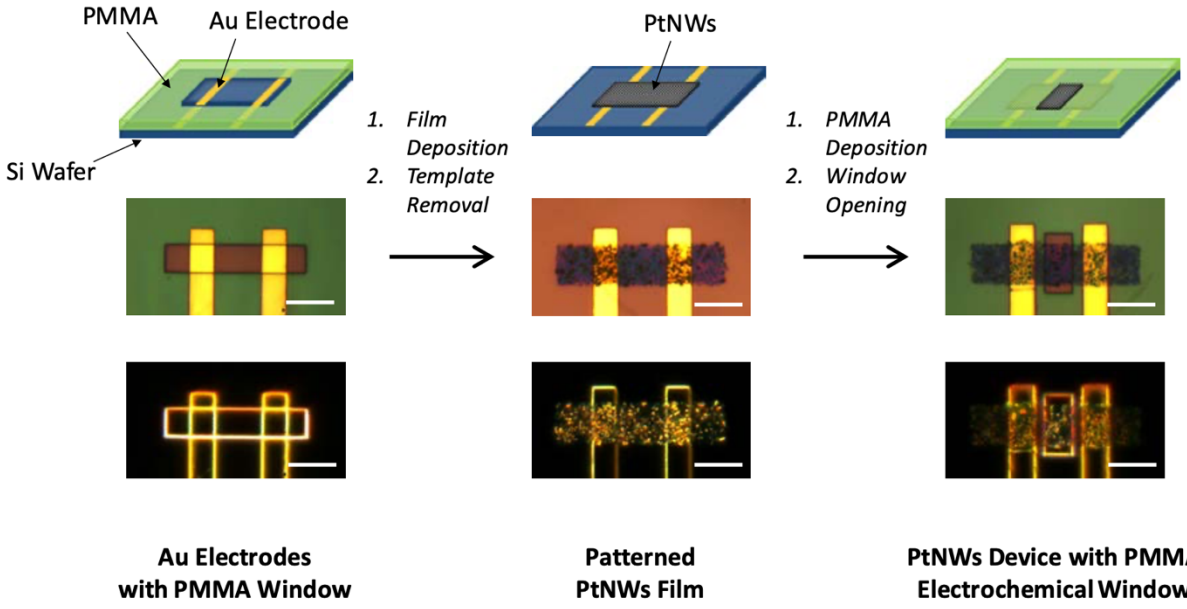

Figure 2-3. Schematic illustration platinum nanowires (PtNWs) device fabrication (depicted at top) for on-chip electrochemical and ETS measurements and corresponding optical images (bright field, middle; dark field, bottom). Scale bars in the optical images are 10 μm. Adapted from reference 4 with copyright permission.

After a 2-hr baking (90 °C), the PMMA layer was removed with acetone and the PtNWs were deposited on the substrate with desired patterns. Before the ETS measurement, another layer of PMMA (~500 nm thick, electrochemically inert) was deposited over the PtNWs device to prevent electrochemical reactions on the Au/Ti electrodes with the solution. E-beam lithography was used to open a small window that only exposes PtNWs to the solution for on-chip electrochemistry and in situ conductance measurement. The final device, with exposed PtNWs and PMMA protected electrodes was used for in-device electrochemistry and in situ electrical transport spectroscopy, which will be introduced in detail in the next section.

2.3 On-chip electrochemical and electrical transport spectroscopy (ETS) measurements.

A two-channel source-measure unit (SMU, Keysight B2902a) was used for ETS measurements. The first SMU channel was used as a potentiostat to perform the on-chip CV by applying the potential (V_G) of source/drain electrode (acting as working electrode) as to the reference electrode (leak-free Ag/AgCl) while collecting the gate current (I_G) through the counter electrode (Pt wire). In a typical CV measurement, the scan rate is 28 mV/s. The second SMU channel was used to record ETS signals by supplying a small bias potential (50 mV) between source and drain electrodes and collecting the electrical conductive current (I_{SD}), as shown in **Figure 2-4**.

Instead of an open chamber configuration from the original setup of ETS, a microfluidic setup was introduced to achieve more efficient control of the electrolytes exposed to the PtNWs device. A PDMS microfluidic channel was mounted on the Si chip with the channel aligned with the central region where the PtNWs device is located. Polyethylene tubing was attached to the inlet and the outlet holes on the PDMS channel, and $HClO_4$ solutions or mixed electrolytes containing

$HClO_4$ and desired anions (for introducing each anion, the corresponding sodium salt is used) were drawn through the channel using a syringe pump.

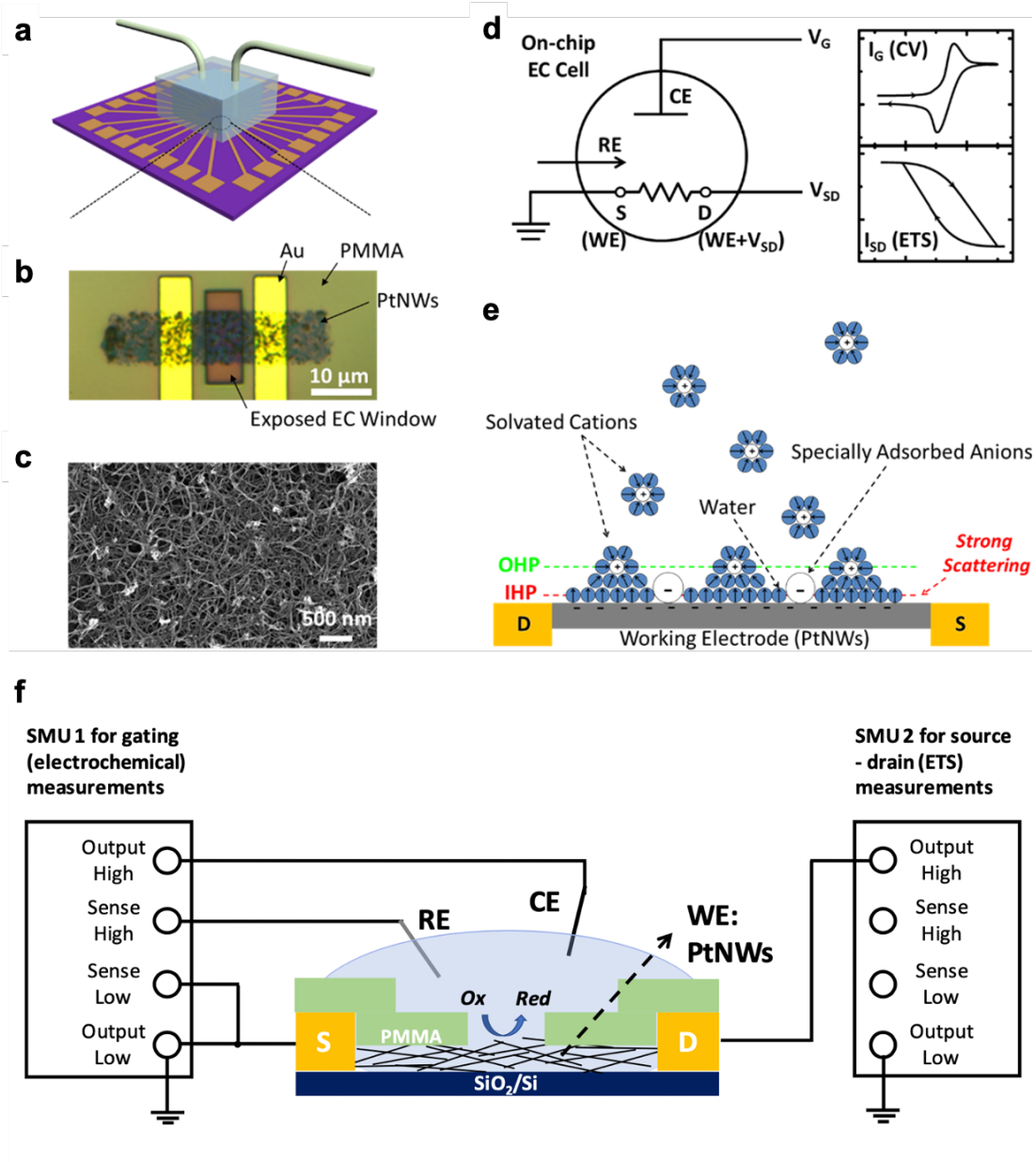

Figure 2-4. Schematic illustration of the experimental setup of in situ electrical transport spectroscopy (ETS) measurement. (a) Schematic illustration of the microfluidic system for the on-chip electro-chemical measurements. (b) Optical microscopic image (OM) of an on-chip cell (enlarged area in a) showing PMMA (electro-chemically inert) covered gold electrodes, and the exposed PtNWs network in the opened PMMA window. (c) SEM image of the PtNWs network. (d) The schematic diagram for the working principles of concurrent CV and ETS. CE, counter electrode; RE, reference electrode; WE, working electrode; S, source;

D, drain. (e) Schematic illustration of the double layer model for PtNW electrode in an aqueous electrolyte with specific adsorption of anions at the inner Helmholtz plane (IHP). (f) Schematic illustration of the connection and configuration for on-chip electrochemical and ETS measurements.

The typical flow rate was 1 $mL \cdot h^{-1}$ during ETS tests and 10 $mL \cdot h^{-1}$ for the electrolyte switching. All electrolytes were degassed with ultrahigh purity nitrogen before use. For surface cyanide modification, the electrochemically cleaned PtNW devices were exposed to 0.1 M KCN solution for 30 min under an open circuit, followed by extensive rinsing with the flow of DI water and then the 0.1 M $HClO_4$ electrolyte. No unexpected or unusually high safety hazards were encountered.

For a typical measurement in this study, the gate (Faradaic) current is generally several orders of magnitude smaller than the ETS current (I_G ~1 nA and I_{SD} ~50 μA). Therefore, the in-device CV current does not affect the ETS current and no additional background subtraction or other mathematical treatment is needed before the data analysis. In the situation (e.g. negative potential below 0 V vs RHE) when electrochemical current I_G is significant enough to affect the source-drain current (I_{SD}), an equivalent circuit can be used to subtract the I_G background from the ETS (I_{SD}) channel, as shown in **Figure 2-5**.

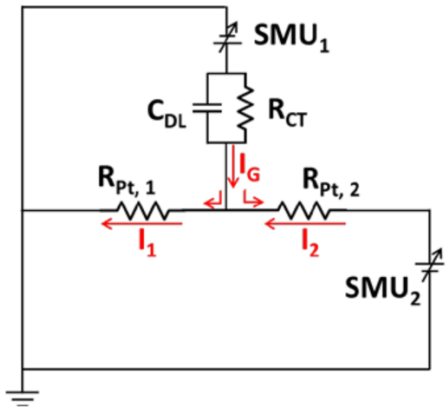

$$I_{sd} = I_2 + I_g/2$$

Figure 2-5. Equivalent circuit model of the ETS measurement. The contributions of gate current to the source-drain current during the measurement can be properly deducted based on the equation provided.

2.4 Normalization of the I_{SD}-V_G results

In an aqueous environment under open circuit, the conduction electrons were at least scattered by surface adsorbed water molecules, and the conductance of PtNWs at this stage can be considered as "baseline" conductive current (I_{SD}^0). This baseline value can be determined before each electrical spectroscopic scan by measuring the I-V characteristics of PtNWs with no V_G applied. With I_{SD}^0 measured, the I_{SD} of each test could also be normalized to relative conductance change ($\Delta I_{SD}/ I_{SD}^0$). This normalization does not change the character of each I_{SD}-V_G curve and makes the comparison between different scans and different devices more reasonable, as the baseline conductance of each device is different and each could drift during measurements, due to the reasons such as Pt atom dissolution. The shape of I_{SD}, G_{SD} and ΔG_{SD} are the same, and in this chapter they are all referred to as ETS results. In the presence of strongly adsorbed anions such as halide, the "baseline" conductive current is also affected by the specially adsorbed anions under the open circuit. Note that in such case the "baseline" surface condition is changing from clean $HClO_4$ to that containing halide anions. Therefore, the comparison of absolute ETS current is more appropriate and more accurate in the study of halide adsorption and is thus adapted in this chapter.

3. Results and discussion

3.1 Sulfate adsorption on the platinum surface

Previously, the surface adsorption of sulfate anions on polycrystalline Pt electrode has been investigated with Fourier transform infrared spectroscopy (FTIR)[8] or sum frequency generation (SFG)[9] in the double layer region at relatively high concentrations (usually in 0.5 M H_2SO_4). Since ETS is a highly surface-sensitive technique, we initiated our measurement at a relatively low concentration. For comparison purposes, the baseline of ETS without the introduction of sulfate

was established in 0.1 M perchloric acid. Based on previous spectroscopy investigation[10], perchlorate ion has been considered as one of the weakest adsorbed anions on platinum. Thus, we chose $HClO_4$ as the acid and background for the investigation of other anion adsorptions.

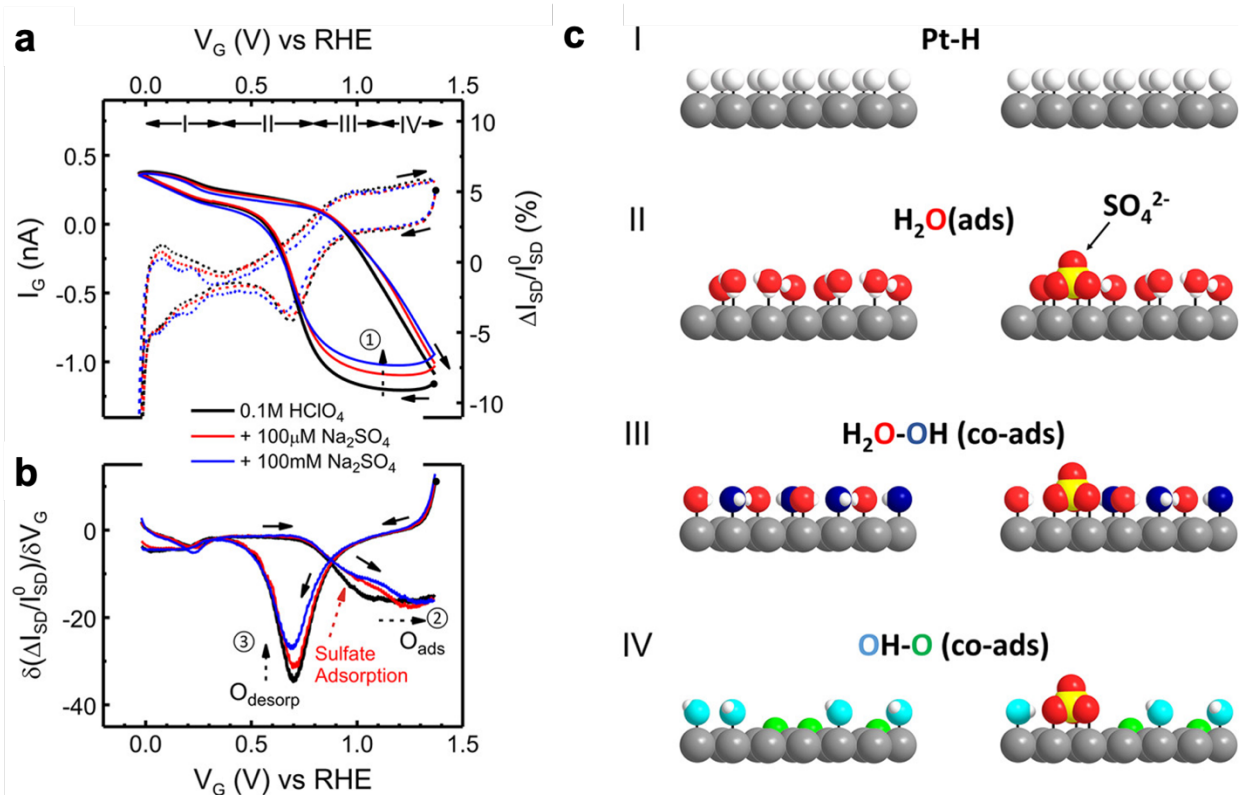

Figure 2-6. In situ electrical transport spectroscopy (ETS) of sulfate adsorption on Pt surface. (a) I_G–V_G (on-chip CV, dashed curves) and normalized I_{SD}–V_G (ETS, solid curves) characteristics of a typical PtNW device in 0.1 M $HClO_4$ (black) and with the addition of varying concentrations of sulfate anions. The CV results resemble the typical CV characteristic of a polycrystalline Pt surface, containing redox regions of under potential hydrogen adsorption (region I); the double layer (region II), reversible adsorption of OH (region III), and surface oxide formation (region IV). (b) Differentiated analysis of ETS (dETS) results showing spectral peak characteristics. Dashed arrows (1 in a and 2, 3 in b) indicate the change of ETS or dETS results by the effect of sulfate adsorption. (c) Schematic models of different Pt surface conditions in different electrochemical regions in $HClO_4$ and with sulfate anions. Pt atoms are gray, H atoms are white, O atoms are red in H_2O_{ads}, blue in OH_{ads}, and green in O_{ads} for a visual guide to the different scattering effects. Solid arrows in all figures indicate the potential sweeping direction, with corresponding dots showing the starting point of the measurement. Adapted from reference 4 with copyright permission.

Figure 2-6a (black curve) shows typical CV and ETS baseline features of the PtNWs, which were introduced in the previous chapter. First, the ETS current remains relatively flat in the double layer (D.L.) region (region II), where the PtNW surface is predominantly occupied by adsorbed water molecules. Second, in the more negative potential range, adsorption/desorption of a monolayer of hydrogen atoms (H_{ads}) on the PtNW surface results in an obvious increase/decrease in the ETS current (region I). The increase in conductance (G_{SD}) during the H adsorption can be attributed to a more predominant specular scattering of electrons (less diffusive scattering) for a Pt−H surface compared to a Pt-H_2O surface. Lastly, when potential is more positive than the double layer region, the adsorption/desorption of surface oxygenated species including hydroxyl groups (region III) and surface oxide(region IV) happens, which caused the current (I_{SD}) to decrease significantly.

The ETS characteristic when sulfate anion is introduced is also presented in **Figure 2-6a**. Our findings show that even though sulfate is considered to be a weakly adsorbed anion, it is still able to alter the overall surface adsorption/desorption cycle of a platinum catalyst even at a relatively low concentration. While there is no obvious difference in the hydrogen adsorption region (region I), the ETS current decreases as the sulfate concentration increases in the double layer region. This indicates sulfate anions, with a stronger scattering effect compared to water molecules, start to adsorb onto the platinum surface. Another obvious change is indicated by arrow ① in the oxide formation region (region IV), during which the conductivity of the device shifts to a higher value when sulfate anions are introduced. Compared to strongly bonded oxygen atoms, sulfated anions have a weaker scattering effect. Thus our observation suggests a small portion of surface oxygenated species are replaced by the adsorbed SO_4^{2-}. Differential analysis of the ETS curve (**Figure 2-6b**) leads to the same conclusion: due to adsorbed sulfate anions, the O_{ads} peak

and the oxide reduction peak both show a decreasing trend in intensity (arrow ② & ③). What's more, the shift of dETS curve in the OH adsorption region (region III) suggests that SO_4^{2-} adsorption occurs through co-adsorption of sulfate and hydroxyl group, and no extra adsorption is observed at potential higher than 1.2V vs RHE. **Figure 2-6c** provides a schematic illustration of different surface environments in the CV cycle with/without sulfate anions.

3.2 Halide adsorption on the platinum surface

It is especially appealing for the in-situ characterization of interface adsorbates without distinct infrared spectroscopic features and those that do not generate specific electrochemical features. For example, halide anions (Cl^-, Br^-, I^-) belong to this category. Due to the abundance of halide in natural and industrial environments, the mechanistic study of the halide adsorption (especially in trace amount) on Pt catalysts is of both fundamental and practical significance. Historically, the lack of intrinsic IR spectroscopic feature made in situ study of halide adsorption relied heavily on X-ray based spectroscopy[11-13] and non-linear optical method of second harmonic generation (SHG)[14]. Sensitivity is usually a challenge for these methods, and the previous investigation was mainly performed at relatively high concentrations (10^{-3} M). With the assistance of ETS, we examined the halide adsorption on the platinum surface in electrolytes containing different concentrations of halides. **Figures 2-7a** shows typical CV characteristics of a PtNWs device with chloride introduced, together with the ETS acquired in the same cycle (**Figure 2-7b**).

Compared with sulfate adsorption, the ETS characteristics of the PtNWs are altered much more significantly by chloride adsorption, particularly considering that the concentration of chloride is about several orders of magnitude smaller than sulfate in the previous section. This result suggests that chloride binds stronger to the platinum surface in a certain potential window.

In the double layer region, a clear drop in ETS current can be observed (indicated by the dashed arrow in region II, **Figure 2-7b**) due to the specific adsorption of Cl_{ads} at the inner Helmholtz plane (IHP), which exhibits a strong scattering effect compared to water molecules. Similar to the trend observed in previous section with sulfate adsorption, the ETS current increases in the region of oxide formation (indicated by the dashed arrow in region IV, **Figure 2-7b**). This observation suggests that the competitive chloride adsorption blocks some portion of oxygen adsorption, resulting in less surface scattering hence better device conductivity.

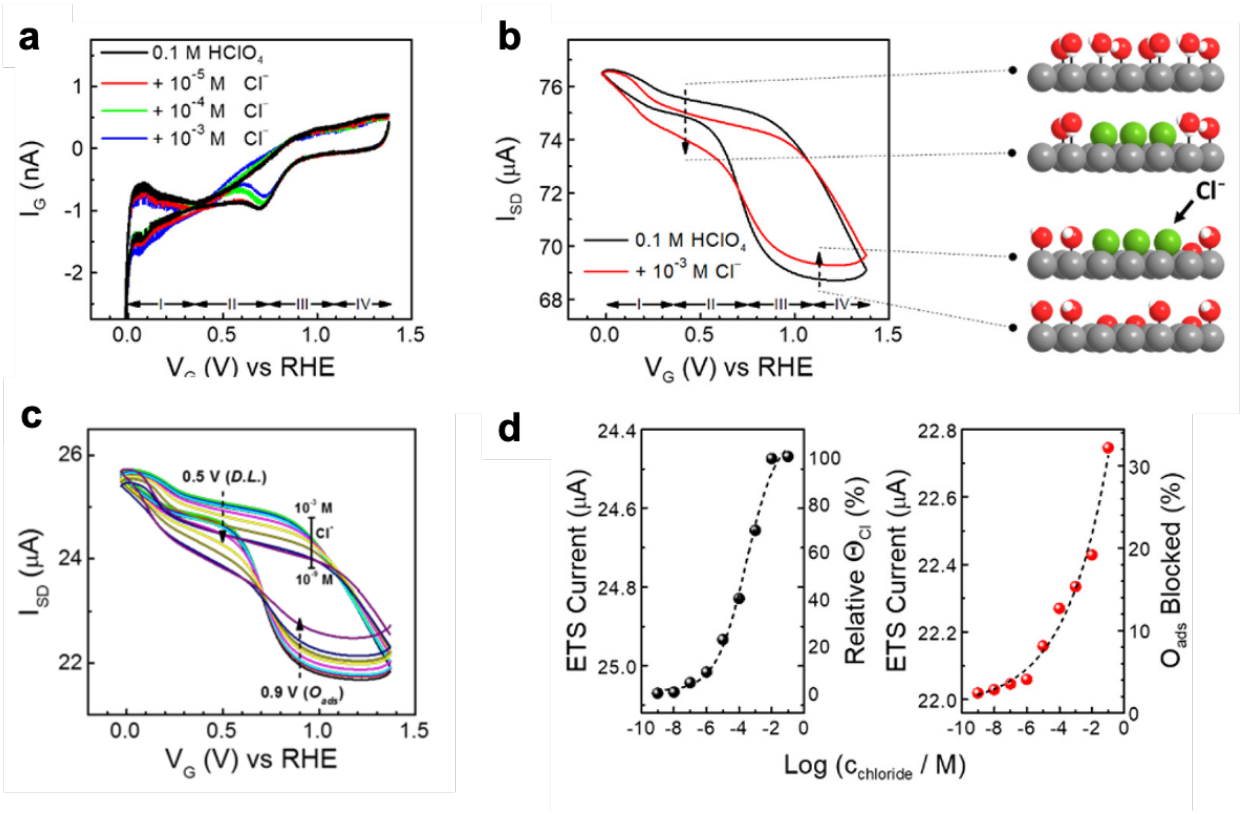

Figure 2-7. In situ ETS study of chloride adsorption on Pt surface. (a) On-chip CV characteristics of a typical PtNWs device in 0.1 M $HClO_4$ (black) and with the addition of varying concentrations of sodium chloride. Redox regions of hydrogen adsorption (region I), the double layer (D.L.) (region II), reversible adsorption of OH (region III), and surface oxide formation (region IV) can be identified. (b) ETS characteristics of a typical PtNWs device in 0.1 M $HClO_4$ (black) and with the addition of 1 mM chloride anions (red). Dashed arrows indicate the change of ETS by the effect of chloride adsorption in the double layer region and oxide formation region. Corresponding schematic representations are shown on the right.

Pt atoms are gray, H atoms are white, O atoms are red, Cl atoms are green. (c) ETS curve of PtNWs device in $HClO_4$ with different concentrations of chloride in the system. (d) ETS current extracted from the curve in D.L. (left, value obtained at 0.5 V vs RHE) and oxidation (right, value obtained at 0.9 V vs RHE) regions at different chloride concentrations. Black dashed curves are sigmoidal (left) and exponential (right) fittings of the current values. Electrically derived surface coverage of Cl_{ads} at the double layer region and percentage of blocked O_{ads} by chloride in oxide formation region are shown on the corresponding right axis. Adapted from reference 4 with copyright permission.

Noticeably, the Cl_{ads} in the double layer region lowers down the current baseline, which resulted in a larger change in ETS signal of the H_{upd} region. The similar maximum ETS current at the end of H_{upd} potential indicates the complete removal of adsorbed chloride by hydrogen atoms over the Pt surface. Besides, no additional "step" in ETS was observed here, indicating a gradual replacement of Cl_{ads} by H_{ads} with the negative-going potential sweep. We would also like to point out that the enlarged response in H_{upd} and a dropped current with a slightly increased slope in D.L. resembles the ETS shape of the first published work about this method[6]. The result we have here indicates that the platinum nanowire's ETS characteristics we established before were contaminated by a trace amount of chloride from the reference electrode. Compared to the original setup of ETS, we replaced the glass body Ag/AgCl reference with a leakless Ag/AgCl reference electrode which has negligible electrolyte leakage during the measurements presented here.

In addition to qualitative analysis, we carried out a series of ETS measurements when different concentrations of sodium chloride are introduced into the solution (**Figure 2-7c**) and we further utilized these results to obtain quantitative information on chloride adsorption at the PtNWs surface. Results shown in **Figure 2-7d** are obtained from the ETS curve in **Figure 2-7c** at the potential of 0.5 V vs. RHE (corresponding to the D.L. region) and 0.9 V vs. RHE (corresponding to the O_{upd} region, which is a key indicator for the electrokinetics during ORR). Quantitative analysis of ETS currents shows adsorption kinetics of chloride at specific potentials, with an

electrically determined surface coverage of Cl_{ads} (in D.L., **Figure 2-7d** left) and blockage of oxygen adsorption (in O_{upd}, **Figure 2-7d** right). As shown in **Figure 2-7d**, Cl^- coverage significantly increases at the onset concentration of approximately 1 μM in both regions. Interestingly, at high concentrations, Cl^- adsorption shows a different behavior: while saturated coverage of Cl_{ads} was achieved at ~10 mM at double layer, continuously increased blocking of the O_{ads} site is observed with increasing concentrations of Cl^- in the O_{upd} region. These results presented here agree well with those derived from SHG (D.L.)[14] and electrochemical (O_{upd})[15] measurements, and demonstrate a quantitative approach that works for the entire potential window, with better sensitivity and accuracy for the characterizations of low concentration of target analyte.

Besides chloride adsorption, we further investigated the adsorption feature of bromide and iodide on a platinum surface. The ETS and corresponding dETS results from the same PtNWs device are presented in **Figure 2-8**. For bromide anion, its adsorption results in a qualitatively similar yet much stronger ETS signal change on PtNWs to that of Cl_{ads}, with a more pronounced drop of ETS current in the double layer region, an increase of ETS current in the oxide formation region, elongated ETS change in the H_{upd} region, along with a corresponding H_{upd} peak increase/O_{ads} shift in dETS results. The qualitatively similar yet quantitatively stronger ETS signal variation from Br_{ads} is consistent with a stronger binding of bromide to Pt surface compared with chloride. As for iodide adsorption on platinum, it is commonly known that at an irreversibly adsorbed zerovalent iodine monolayer is formed on the Pt surface upon exposure to iodide anions which remains stable over a wide potential range and strongly inhibits the hydrogen and oxygen adsorption on the Pt surface[14]. Such characteristic results in a 'flat' ETS and dETS curve in iodide-containing condition, with negligible amount of hydrogen adsorption at relatively low potential range.

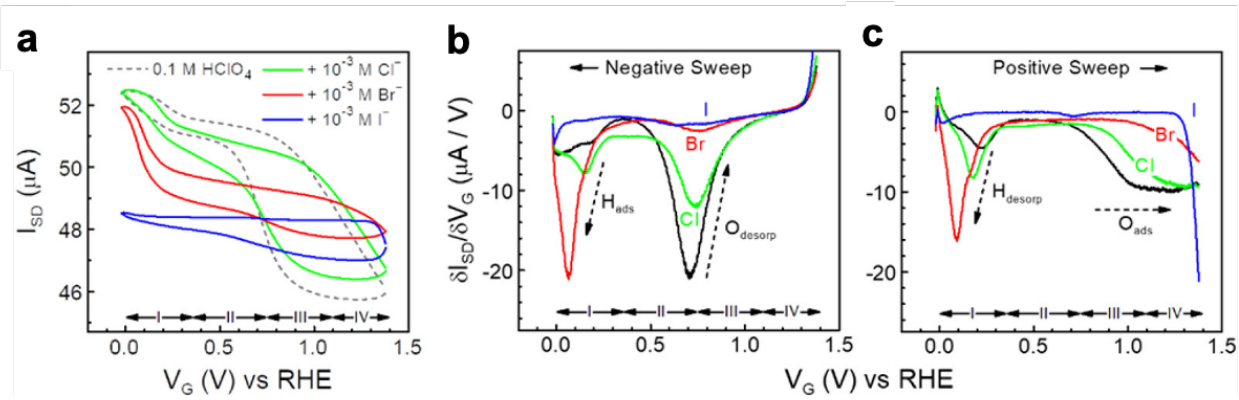

Figure 2-8. In situ ETS study of halide adsorption on Pt surface. (a) ETS characteristics of a typical PtNW device in 0.1 M HClO4 (dashed black, as baseline comparison) and with addition of 1 mM chloride (green), bromide (red) and iodide (blue) anions. (b,c) dETS characteristics of halide adsorptions results from negative (b) and positive (c) going potential sweep are divided for the clarity of comparison. Adapted from reference 4 with copyright permission.

The evolution of ETS characteristics for halide anions is consistent with their binding strength: $Cl^- < Br^- < I^-$, each with unique features that reveal the in situ surface processes in detail. Interestingly, the ETS signals of Cl_{ads} show a slight but obvious potential dependence in the double layer region, i.e., a slightly increased slope in ETS and an elevated peak level in dETS (**Figure 3b,c**), whereas Br_{ads} and I_{ads} show a relative flat (potential independent) feature. These results indicate that in the D.L. region, the surface adsorption (coverage) of Cl_{ads} gradually changes with the applied gate potential, while the adsorption layer for bromide and iodide is relatively stable and potential independent. The potential dependence of halide adsorption found previously in this specific region has received conflicting conclusions from different spectroscopic and electrochemical studies[14] and our ETS investigation provides important experimental evidence and additional insights to resolve these controversies.

3.3 Anionic competition on the platinum surface

We further investigated chloride adsorption in competitive environments in order to establish its relationship with the electrokinetics of platinum-catalyzed ORR. As demonstrated by ETS studies in previous sections, the presence of sulfate or chloride anions (even at low concentrations) severely impedes the surface adsorption of O species, which may influence the overall ORR kinetics on Pt-based catalysts. We measured the polarization curves for Pt/C catalyzed ORR obtained in a rotating disk electrode (RDE) in clean and Cl^- contaminated electrolytes, which is presented in **Figure 2-9a**. The ORR activity of Pt/C indeed shows a significant decay with increasing concentrations of Cl^-. The increased overpotential in the presence of Cl^- is consistent with the site-blocking of oxygen adsorption by Cl_{ads} observed in ETS studies (**Figure 2-7**).

To address such chloride poisoning effect for Pt-catalyzed ORR performance, Cl^- inhibition is much needed yet extremely challenging, as chloride adsorption is much stronger on the Pt surface, and the influence of Cl_{ads} starts at a much lower concentration (~ 10^{-6} M). Importantly, the ability of ETS to provide highly sensitive, in operando, and surface specific characterization of Cl^- adsorption provides a highly efficient pathway to explore possible approaches to address this issue from a fundamental perspective. Using ETS as an effective probe, we demonstrated two types of anodic competition for chloride adsorption: a "static" anionic cyanide adlayer, and a "dynamic" high ionic strength electrolyte (high concentration of perchloric anions).

Cyanide (CN^-) adsorbs irreversibly on the Pt surface and forms a stable and relatively inert adlayer. Due to the unique molecular patterns of CN_{ads} on the Pt(111) surface, it has been successfully applied to provide fundamental insights into different electrocatalytic reactions[16, 17].

We investigated the general adsorption feature of cyanide on the platinum surface with ETS measurements (**Figure 2-9b**). Interestingly, the overall device conductivity drops sharply after the introduction of CN^-, but the ETS curve after normalization remains mostly unchanged compared to the result of clean PtNW surface. We can therefore conclude that while CN_{ads} blocked the surface Pt atoms onto which they adsorb, the CN-free sites on the Pt surface are unaffected for the adsorption of H, H_2O, and O species. This characteristic is entirely different from that of other strong binding molecules such as bromide, iodide from the previous section. The above hypotheses have been previously proposed to explain the catalytic performance of cyanide modified platinum electrodes[18] and our ETS characterization here provides straightforward experimental support.

To examine the viability of the second strategy, the Cl^- adsorption was further probed under a high concentration of perchloric anions (considered one of the weakly adsorbed anions on Pt), to understand how weakly adsorbed anions can affect the strongly adsorbed anions at a huge concentration difference. **Figure 2-9d,e** depicts the ETS and dETS results of PtNWs in the presence of Cl^- with high concentrations of ClO_4^- (0.4 M). Comparing the ETS and dETS data obtained in electrolyte with a high concentration of ClO_4^- (0.4 M) with or without the presence of low-level Cl^- (10 μM), it is apparent that the influence of Cl^- is negligible (no obvious O_{ads} overpotential, no current level change in the O_{upd} region, as indicated by dashed arrows in **Figure 2-9d,e**), in stark contrast to the test conducted in electrolyte with only 0.1M $HClO_4$. This observation suggests that the competitive adsorption of highly concentrated ClO_4^- is also increasing the chloride resistance of the platinum surface. However, such behavior only occurs at 10 μM of Cl^-; concentrations higher than 100 μM Cl^- still show influence on the surface adsorption processes on Pt with the same perchlorate anion concentration, which can be confirmed by the dETS results in **Figure 2-9f**.

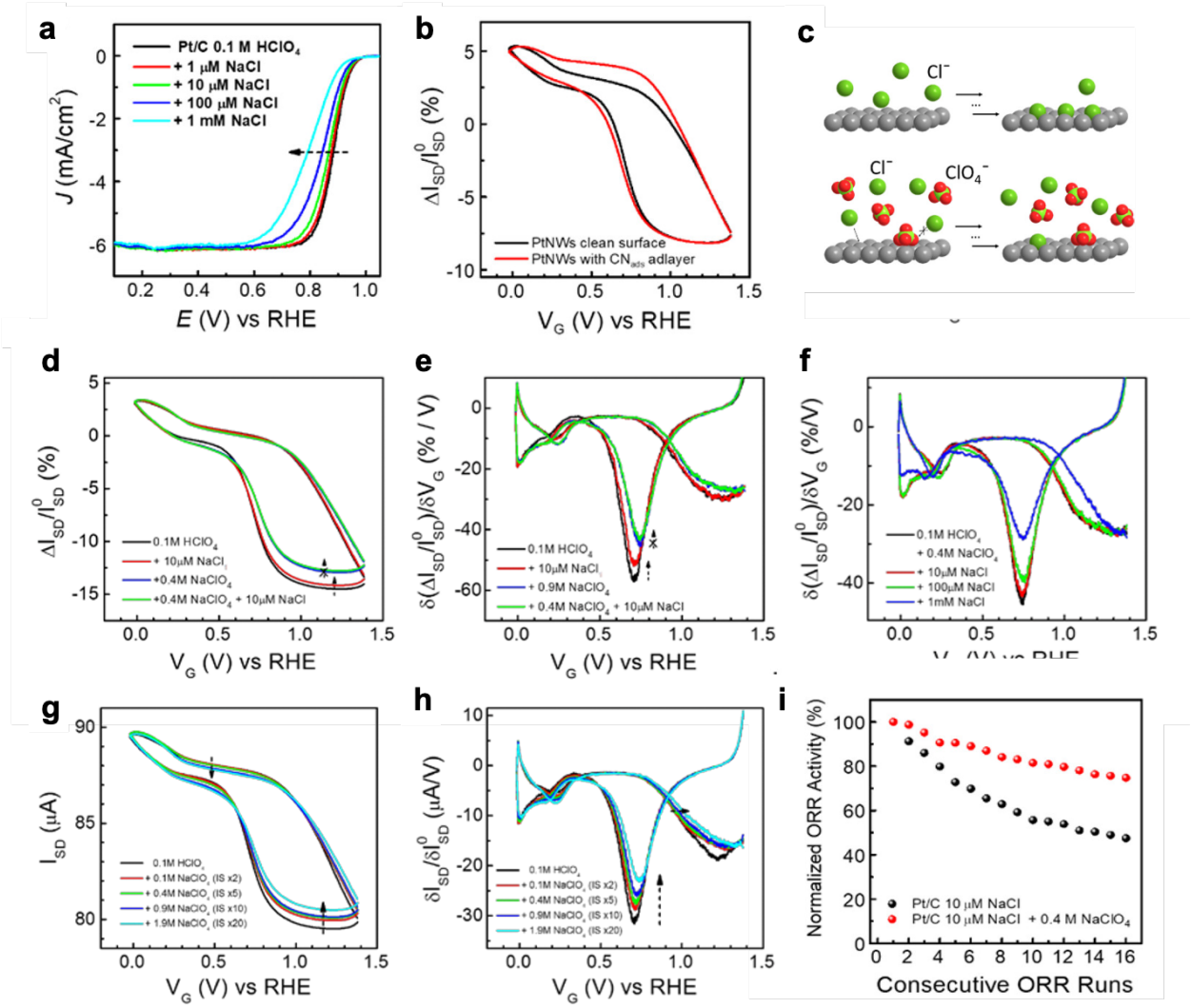

Figure 2-9. Electrical transport spectroscopy (ETS) of perchloride adsorption and competition with chloride on Pt surface. (a) Oxygen reduction reaction (ORR) polarization curves of commercial Pt/C on a rotating disk electrode (RDE) in $HClO_4$ (0.1 M) and with varying concentrations of Cl^-. (b) ETS characteristics of clean PtNW device (black) and PtNWs modified by a surface cyanide adlayer (red) in 0.1 M $HClO_4$. (c) Schematic illustration of enhanced Cl^- resistance through "dynamic" competitive surface adsorption. Cl^- accumulation is suppressed by a high concentration of perchloride anions. Pt atoms are grey, O atoms are red, and Cl atoms are dark green. (d, e) ETS (d) and dETS (e) characteristics of Cl^- (10 μM) adsorptions on PtNWs in 0.1 M $HClO_4$ (black to red) and 0.1 M $HClO_4$ + 0.4 M $NaClO_4$ (blue to green). Dashed arrows show the lack of Cl_{ads} features in 0.4 M $NaClO_4$ containing electrolyte. (f) ETS characteristics of PtNWs in 0.1M $HClO_4$ with addition of 0.4 M perchloride anions (black) and 10 μM, 100 μM and 1 mM of Cl^-. (g,h) ETS (g) and dETS (h) characteristics of a typical PtNWs device in 0.1 M $HClO_4$ (black) and with addition of varying concentrations (from 0.1M to 1.9M) of perchloride anions. Dashed

arrows indicate the change of ETS or dETS results by the effect of perchloride adsorption. The ETS results reveal that even though it has been identified as a weakly adsorbed anion, high concentrations of ClO_4^- still show adsorption on the platinum surface, causing anionic competition in the O_{upd} region. (i) Evolution of ORR activities of Pt/C over consecutive runs (stability tests) in Cl^- (10 μM) contaminated electrolytes with or without high concentration (0.4 M) of $NaClO_4$. Adapted from reference 4 with copyright permission.

Even though the competitive adsorption of highly concentrated ClO_4^- might result in a negative effect toward reaction kinetics (**Figure 2-9g,h**), it is still possible to offer other benefits. As shown in **Figure 2-9i**, for Pt-catalyzed ORR, not only does Cl^- contamination increase the overpotential and reduce the current density, it also shows an accumulating effect that continuously poisons the catalyst's ORR performance over time. This effect could potentially cause serious activity degradation over time and thus a long-term durability problem to real-world device like polymer exchange membrane fuel cells (PEMFCs)[19]. By introducing a high concentration of ClO_4^-, the current drop over consecutive tests in Cl^- containing electrolytes is greatly reduced. Through our interfacial study, we have discovered a novel anion competition mechanism that significantly reduces the accumulation of halide adsorption on the Pt surface. It therefore offers a promising solution, by simply optimizing the electrolyte content, to increase the impurity tolerance of fuel cell devices and their long-term durability.

4. Conclusion

With the direct experimental evidence derived from a unique nanoelectronic measurement--ETS, we have investigated the surface adsorption features of various anions (such as sulfate, halides, and cyanides) on the platinum catalyst, and demonstrated quantitatively that the competitive anionic adsorption can have a profound effect on ORR activity. The combination of electrochemical and nanoelectronic measurements produces highly sensitive and surface-specific signals for exploring electrochemical interfaces with considerable precision and accuracy,

allowing for the first time both qualitative and quantitative analysis at a low level of target analytes. It is especially efficient for the in situ characterization of surface adsorbed anions without distinct infrared spectroscopic features (such as halides), and those that do not generate specific electrochemical features (e.g., CV peaks). For similar reasons, this on-chip approach is also appealing for the electrochemical interface that involves cations, which tailor the ORR activities via noncovalent interactions with surface oxygenated species yet are extremely difficult to study for their lack of spectroscopic feature[20-23].

The unique adsorption kinetics of each anion tested in this work and its influence on the corresponding oxygen species are used to rationalize the dependency of important Pt-catalyzed reactions (such as ORR) on anionic contamination. Based on the ETS descriptor for the ORR performance, we further investigated the chloride poisoning behavior in more complex anionic environments and demonstrate potential strategies to mitigate the poisoning effect using either a "static" anionic cyanide adlayer (that could hinder Cl^- adsorption and reduce the Cl_{ads} induced overpotential) or a "dynamic" high ionic strength approach (that helps prevent the long-term accumulation of Cl^- poisoning) for improved efficiency and stability of real-world energy conversion devices.

5. Reference

1. Wang, C.; Markovic, N. M.; Stamenkovic, V. R., Advanced platinum alloy electrocatalysts for the oxygen reduction reaction. *Acs Catalysis* **2012,** *2* (5), 891-898.

2. Wu, J.; Yang, H., Platinum-Based Oxygen Reduction Electrocatalysts. *Accounts of Chemical Research* **2013,** *46* (8), 1848-1857.

3. Bartholomew, C. H.; Farrauto, R. J., *Fundamentals of industrial catalytic processes*. John Wiley & Sons: 2011.

4. Ding, M.; Zhong, G.; Zhao, Z.; Huang, Z.; Li, M.; Shiu, H.-Y.; Liu, Y.; Shakir, I.; Huang, Y.; Duan, X., On-Chip in Situ Monitoring of Competitive Interfacial Anionic Chemisorption as a Descriptor for Oxygen Reduction Kinetics. *ACS Central Science* **2018,** *4* (5), 590-599.

5. Xia, B. Y.; Wu, H. B.; Yan, Y.; Lou, X. W.; Wang, X., Ultrathin and Ultralong Single-Crystal Platinum Nanowire Assemblies with Highly Stable Electrocatalytic Activity. *Journal of the American Chemical Society* **2013,** *135* (25), 9480-9485.

6. Ding, M.; He, Q.; Wang, G.; Cheng, H.-C.; Huang, Y.; Duan, X., An on-chip electrical transport spectroscopy approach for in situ monitoring electrochemical interfaces. *Nature Communications* **2015,** *6*, 7867.

7. Ding, M.; Liu, Y.; Wang, G.; Zhao, Z.; Yin, A.; He, Q.; Huang, Y.; Duan, X., Highly sensitive chemical detection with tunable sensitivity and selectivity from ultrathin platinum nanowires. *Small* **2017,** *13* (5), 1602969.

8. Su, Z.; Climent, V.; Leitch, J.; Zamlynny, V.; Feliu, J. M.; Lipkowski, J., Quantitative SNIFTIRS studies of (bi)sulfate adsorption at the Pt(111) electrode surface. *Physical Chemistry Chemical Physics* **2010,** *12* (46), 15231-15239.

9. Braunschweig, B. r.; Mukherjee, P.; Dlott, D. D.; Wieckowski, A., Real-time investigations of Pt (111) surface transformations in sulfuric acid solutions. *Journal of the American Chemical Society* **2010,** *132* (40), 14036-14038.

10. Iwasita, T.; Xia, X., Adsorption of water at Pt(111) electrode in HClO4 solutions. The potential of zero charge. *Journal of Electroanalytical Chemistry* **1996,** *411* (1), 95-102.

11. Arruda, T. M.; Shyam, B.; Ziegelbauer, J. M.; Mukerjee, S.; Ramaker, D. E., Investigation into the Competitive and Site-Specific Nature of Anion Adsorption on Pt Using In Situ X-ray Absorption Spectroscopy. *The Journal of Physical Chemistry C* **2008,** *112* (46), 18087-18097.

12. Russell, A. E.; Rose, A., X-ray Absorption Spectroscopy of Low Temperature Fuel Cell Catalysts. *Chemical Reviews* **2004,** *104* (10), 4613-4636.

13. Magnussen, O. M., Ordered Anion Adlayers on Metal Electrode Surfaces. *Chemical Reviews* **2002,** *102* (3), 679-726.

14. Campbell, D. J.; Lynch, M. L.; Corn, R. M., Second harmonic generation studies of anionic chemisorption at polycrystalline platinum electrodes. *Langmuir* **1990,** *6* (11), 1656-1664.

15. Novak, D. M.; Conway, B. E., Competitive adsorption and state of charge of halide ions in monolayer oxide film growth processes at Pt anodes. *Journal of the Chemical Society, Faraday Transactions 1: Physical Chemistry in Condensed Phases* **1981,** *77* (10), 2341-2359.

16. Ciapina, E. G.; Lopes, P. P.; Subbaraman, R.; Ticianelli, E. A.; Stamenkovic, V.; Strmcnik, D.; Markovic, N. M., Surface spectators and their role in relationships between activity and selectivity of the oxygen reduction reaction in acid environments. *Electrochemistry Communications* **2015,** *60*, 30-33.

17. Cuesta, A., At least three contiguous atoms are necessary for CO formation during methanol electrooxidation on platinum. *Journal of the American Chemical Society* **2006,** *128* (41), 13332-13333.

18. Strmcnik, D.; Escudero-Escribano, M.; Kodama, K.; Stamenkovic, V. R.; Cuesta, A.; Marković, N. M., Enhanced electrocatalysis of the oxygen reduction reaction based on patterning of platinum surfaces with cyanide. *Nature chemistry* **2010,** *2* (10), 880-885.

19. Ehteshami, S. M. M.; Taheri, A.; Chan, S., A review on ions induced contamination of polymer electrolyte membrane fuel cells, poisoning mechanisms and mitigation approaches. *Journal of industrial and engineering chemistry* **2016,** *34*, 1-8.

20. Dunwell, M.; Wang, J.; Yan, Y.; Xu, B., Surface enhanced spectroscopic investigations of adsorption of cations on electrochemical interfaces. *Physical Chemistry Chemical Physics* **2017,** *19* (2), 971-975.

21. Chen, X.; McCrum, I. T.; Schwarz, K. A.; Janik, M. J.; Koper, M. T., Co-adsorption of cations as the cause of the apparent pH dependence of hydrogen adsorption on a stepped platinum single-crystal electrode. *Angewandte Chemie International Edition* **2017,** *56* (47), 15025-15029.

22. Berkes, B. z. B.; Inzelt, G. r.; Schuhmann, W.; Bondarenko, A. S., Influence of Cs+ and Na+ on specific adsorption of* OH,* O, and* H at platinum in acidic sulfuric media. *The Journal of Physical Chemistry C* **2012,** *116* (20), 10995-11003.

23. Strmcnik, D.; Van Der Vliet, D.; Chang, K.-C.; Komanicky, V.; Kodama, K.; You, H.; Stamenkovic, V.; Markovic, N., Effects of Li+, K+, and Ba2+ cations on the ORR at model and high surface area Pt and Au surfaces in alkaline solutions. *The Journal of Physical Chemistry Letters* **2011,** *2* (21), 2733-2736.

Chapter 3. ETS investigation of Platinum Surface Hydronium's pKa and Its Impact on Hydrogen Evolution Reaction

1. Introduction and background

The Platinum group metal catalysts play an essential role in electrochemical energy conversion and storage, a field of central importance to the advancement of various renewable energy technologies[1-4]. A fundamental understanding of the molecular structures of the electrochemical interfaces and their role in governing the heterogeneous electrocatalytic reaction rates are essential for developing future generations of electrocatalysts with improved catalytic activity and stability for variable relevant electrochemical reactions, including hydrogen evolution reactions (HER) [5, 6]. To this end, various *in situ* characterizations, including X-ray based spectroscopy as well as vibrational spectroscopies including Fourier transform infrared (FTIR), sum-frequency generation (SFG) and Raman spectroscopy[7-13], and advanced simulations have been developed for probing and understanding the complex interfacial molecular structures of electrode/electrolyte interfaces.

The central role of water in aqueous phase electrochemistry, which didn't receive enough attention in the past, is receiving increasing recently interest[6, 14]. It forms the electric double layer, determines solute/electrode association, and in some situations can accept and donate electrons. While the potential dependence of interfacial water structure has been extensively explored, the effect of pH, especially in acidic condition when hydronium ions (H_3O^+) are dominant, is not well understood[15, 16]. The investigation of hydronium ions on metal surfaces was first conducted by simulating the electrochemical double layer in ultrahigh vacuum (UHV). Wagner and Moylan reported H_3O^+ formation from H(ad) and H_2O(ad) coadsorbed on a Pt(111) surface by using high-resolution electron energy loss spectroscopy (HREELS)[17]. Hydronium ions coadsorbed with

bisulfate anions were detected by infrared reflection absorption spectroscopy (IRAS) on Pt(111)[18, 19]. More recently, surface-enhanced infrared absorption spectroscopic (SEIRAS) study also reported observation of the bending mode from adsorbed hydronium at low potential on Au surface[20]. In parallel, the structure of hydronium/hydrated proton clusters on metal/solution interface has also been studied by several theoretical methods based on density functional theory (DFT) and molecular dynamics[21-25].

Despite the spectroscopic and theoretical investigations mentioned above, it remains elusive how bulk environment, including solution pH and electrode potential, may affect the density/distribution of hydroniums near the surface, and how the surface adsorbed hydroniums affect the interfacial structure and the role they play in the relevant electrochemical reactions. Previous simulations have shown that the excess protons preferentially adsorb to a water-platinum interface[26, 27], or hydroniums tend to enrich near water-platinum interface[28]. These studies suggest that the surface water molecules more tend to stay in the protonated status than the bulk water molecules. In other words, the surface hydroniums (H_3O^+) exhibit higher pK_a than the bulk H_3O^+ far away from the surface (pK_a=0). However, a direct probing of the surface water protonation status and confirmation of such theoretical predictions with spectroscopic studies has been difficult due to inevitable convolution with near surface or bulk water signals.

Here in this chapter, we exploit the electrical transport spectroscopy (ETS) approach again for highly specific probing surface water structure on platinum nanowire (PtNWs) under controlled potential in a wide pH range. The ETS signal shows a distinct pH dependence with a sharp switch at a critical point, closely resembling a typical titration curve. The pH-dependent switch in ETS signal can be well fitted by the classic Henderson–Hasselbalch equation with a pKa of 4.3, confirming the surface hydronium exhibits a distinct pK_a from that of bulk (pK_a = 0).

The surface hydronium pKa and surface water protonation fundamentally dictate the pH-dependent HER kinetics. A close analysis of HER under different pH reveals a systematic evolution of the Tafel slopes, with a low Tafel slope around 30 mV/decade from pH 0-2, which gradually increases to 40 mV/decade at pH 3, and then quickly switches to a much higher value of ~120 mV/decade at pH 4.5 or above, showing a similar trend to protonation/deprotonation process and suggesting distinct reaction pathways below and above surface pKa. At a pH below surface hydronium pKa, the surface water molecules are largely protonated, with a rich proton supply for H-adsorption in Volmer step, leading to a typical low Tafel slope of 30 mV/decade; while at higher pH above the surface pKa, there is negligible surface hydronium, the H-adsorption is dictated by water dissociation, leading to much higher over-potential and much larger Tafel slope of 120 mV/decade. These results pave the way towards a more complete understanding of pH effects on the surface water structure and their critical role in the relevant electrochemical reactions and energy conversion processes.

2. Materials and methods

The platinum nanowire preparation and device fabrication process is mostly the same as introduced in the previous chapter. However, several improvements to the microfluidic system and the measurement setup were made to achieve a more reliable ETS signal and to secure the stability of PtNWs device over a long testing period. These improvements will be elucidated in the following sections.

2.1 Improvement to the microfluidic chamber

Compared to the ETS setup in the previous chapter which features a microfluidic system, we improved the design for the PDMS chamber. The new chamber structure enables the Pt counter

electrode (CE) and the ET072-1 leakless Ag/AgCl reference electrode (RE) to be inserted into the chamber through 2 specific holes (**Figure 3-1a**). Securing the CE and RE at a certain location closer to the device can decrease the solution resistance and increase the signal-to-noise ratio. Besides, less adjustment during the solution switching process prevented the disturbance to the PtNWs device.

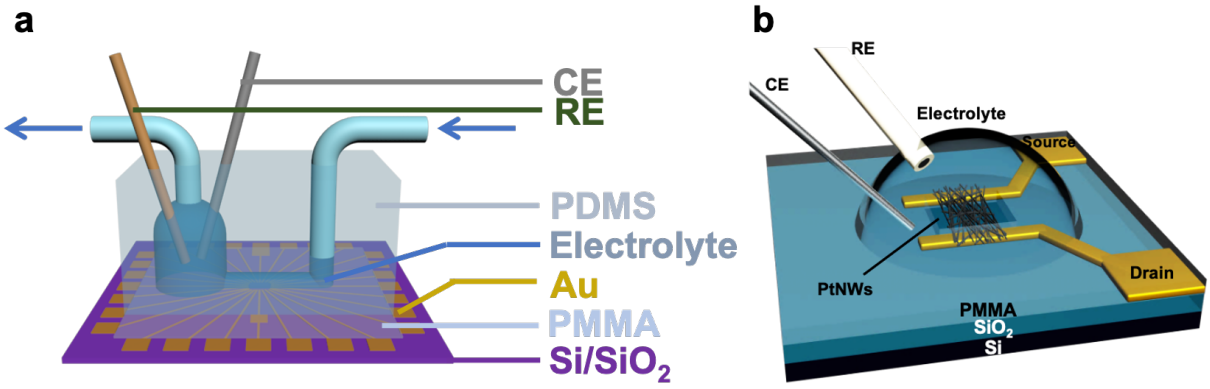

Figure 3-1. Schematic illustration of the updated experimental setup for ETS measurement. (a) Schematic diagram for the microfluidic chamber of ETS, arrows indicate the flow direction of solution. CE, counter electrode; RE, reference electrode; WE, working electrode. (b) Schematic illustration of the device configuration showing PMMA (electrochemically inert) covered gold electrodes, and the exposed PtNWs network in the opened PMMA window.

The $HClO_4$ solution and solutions with different pH were drawn through the channel using a syringe pump. All electrolytes were degassed with ultrahigh purity nitrogen throughout the entire testing process. To ensure the stability of PtNWs device, the typical flow rate was kept at 2 $mL \cdot h^{-1}$ during ETS tests and 8 $mL \cdot h^{-1}$ for electrolyte switching.

2.2 Improvement to the setup of electrical transport spectroscopy (ETS) measurements.

Compared to the previous setup utilizing both channels from one source-measure unit (SMU), a two-channel source-measure unit (SMU, Keysight B2902a) and a lock-in amplifier

(SR830, Stanford Research System) were used for ETS measurements in this chapter. One SMU channel was used as a potentiostat to perform the on-chip CV by applying the gate potential (V_G) of the source/drain electrode (working electrode) as to the reference electrode (Ag/AgCl) while collecting the gate current (I_G) through the counter electrode (Pt), as shown in **Figure 3-2**. The scan rate for CV measurement is 50 $mV \cdot s^{-1}$. The lock-in amplifier provides an AC bias I_{rms}=10 μA with an AC frequency of 1.117kHz, and the voltage on PtNWs device was collected through another SMU channel for conductance calculation. The application of the lock-in amplifier ensures that true conductance of the PtNW device is measured without the interference of the DC leakage current from the gate channel (**Figure 2-5**). Therefore, the on-chip CV current does not affect the ETS signal, and no additional background subtraction or mathematical treatment is needed.

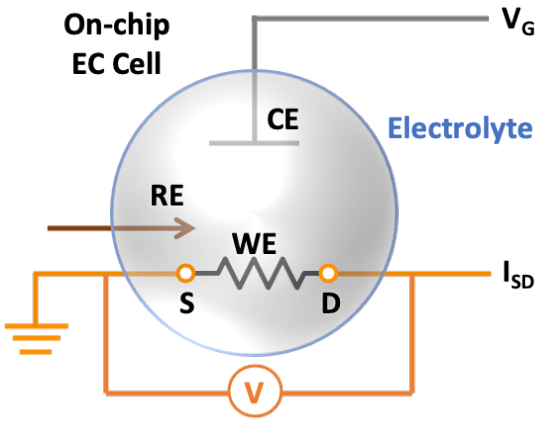

Figure 3-2. Schematic diagram for the working principles of concurrent CV and ETS. CE, counter electrode; RE, reference electrode; WE, working electrode; S, source; D, drain.

2.3 Chemicals

Solutions of different pH values (besides pH=0) were prepared by dilution of 0.10 M $HClO_4$ solution. Different amounts of $KClO_4$ were added to maintain same ionic strength (0.10 M), and the pH was further adjusted with $HClO_4$ or KOH to the desired value. All electrolytes were prepared with Milli-Q water and degassed with ultrahigh purity nitrogen before use.

2.4 Electrochemistry measurement

CV measurements were performed using an electrochemical working station (WaveDriver 200 EIS Bipotentisostat, Pine Instrument). A three-electrode system was employed, using a KCl saturated Ag/AgCl electrode and platinum wire as the reference and counter electrodes. For different pH conditions, the potential of the reference electrode was calibrated in hydrogen saturated electrolyte for conversion to the RHE scale. The disk rotation speed was controlled at 1600 rpm for HER measurement. All of the current densities described in this report are expressed in terms of the geometric electrode surface area. All of the current relationships described have been iR corrected.

3. Results and discussion

3.1 CV and ETS characteristic under different pH

First, we have compared the typical cyclic voltammograms of platinum nanowire with the measured ETS characteristics in the same potential range in unbuffered solution of perchloric acid ($HClO_4$) with pH values of 1, 4 and 7. A certain amount of potassium perchlorate ($KClO_4$) was added to ensure a constant ionic strength for each electrolyte with different pH. In general, the CV plots have distinct characteristic features under different pH (**Figure 3-3a**) and are in good agreement with previous literature report[29]. The information provided by the ETS signal (**Figure 3-3b**) corresponds well with CV measurement. At pH=1, four distinct regions can be observed: the hydrogen adsorption-desorption region (0.05-0.35 V vs. RHE), the double layer region (0.35-0.60 V vs. RHE), the hydroxyl adsorption-desorption region (0.60-1.00 V vs. RHE) and Pt-oxide region (1.00-1.40 V vs. RHE). As for the pH 4 case, while the forward scan of ETS shows similar characteristics to that of pH 1, the backward scan exhibits a distinct two-step feature for oxide

reduction. Due to limited H^+ concentration, the Pt-oxide is only reduced partially in the first step (ca. 1.00-0.60 V vs. RHE) as evidenced by a lesser conductance increase compared to that at pH=1. This can be further confirmed by changing the range of cyclic voltammograms (shown in **Figure 3-8**). The slope of conductance vs. potential varies during the second part of reduction (begins ca. 0.40 V vs. RHE), indicating the existence of additional reduction reaction (underpotential deposition of hydrogen, H-upd) at lower potential. The ETS response for pH 7 shows that Pt-OH_{ad}/O_{ad} formation begins at lower potential (ca. 0.45 V vs. RHE) compared to results in pH 1/pH 4 solution and there is only one peak for their reduction.

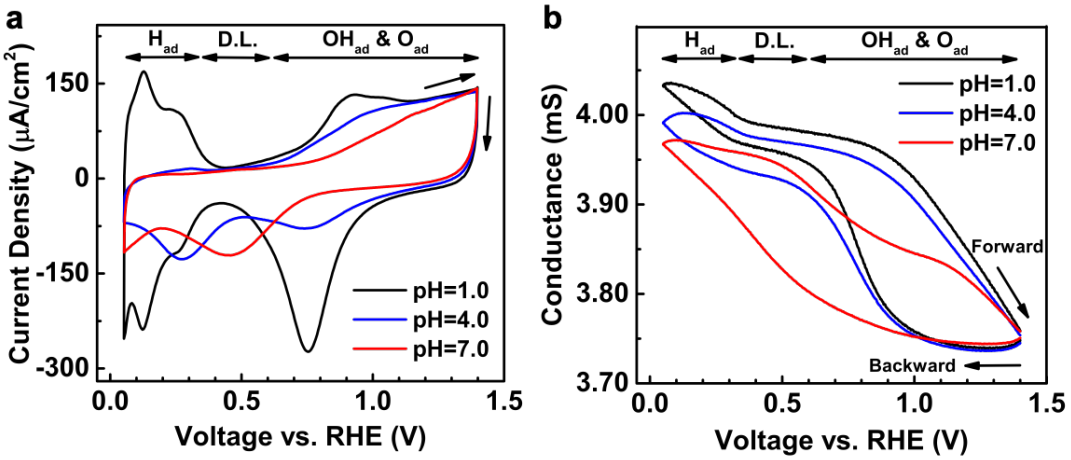

Figure 3-3. In situ electrical transport spectroscopy (ETS) of hydronium adsorption on Pt surface. (a) Cyclic voltammetry of PtNWs in unbuffered solution with pH 1, 4 and 7, with redox regions of hydrogen adsorption/desorption (Had); the double layer (D.L.) and surface oxide formation/reduction region (OHad & Oad). (b) In-situ conductance vs gate voltage relationship of a typical PtNW device in pH 1, 4 and 7 under constant ionic strength (0.10 mol/L). A clear conductance drop can be observed in the double layer region.

To avoid the more complex surface structure evolution in region with Faradaic redox reaction, we focus our attention on the double layer region (0.35-0.60 V vs. RHE) where there is not Faradaic reaction. In the double-layer region, we should expect a flat ETS signal (no conductance change) since the surface adsorbates remain to be water in the entire double potential

range. Nonetheless, a clear slope is observed in the ETS signal in this regime (**Figure 3-3b**), which might be attributed to continued oxidation of incompletely desorbed H (in the forward scan) or continued reduction of the incompletely reduced hydroxide (in the backward scan) on Pt surface. Additionally, it is still apparent the overall conductance of PtNWs in the double layer regime are higher in lower pH solution.

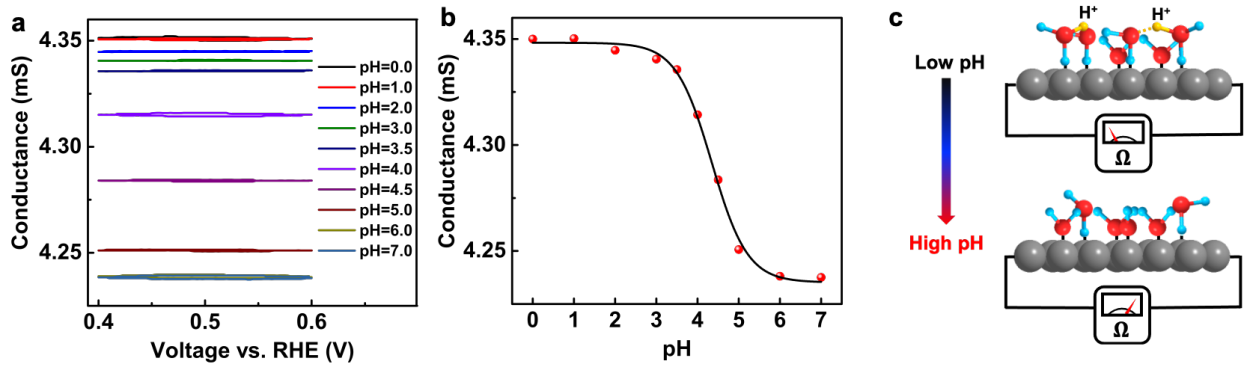

Figure 3-4. In situ electrical transport spectroscopy (ETS) of hydronium adsorption on Pt surface. (a) Conductance of a typical PtNWs device under controlled potential in varying concentrations of perchloric acid under constant ionic strength (0.10 mol/L). (b) Conductance vs pH relationship of a typical PtNWs device in pH 0-7. The black curve is sigmoid fitting of the conductance data based on the Henderson-Hasselbalch equation. (c) Schematic model representing structure change of surface water caused by hydronium ions.

Considering such ETS signal in the double layer regimes is still convoluted with the reside redox reaction in such a large potential sweeping range, we have narrowed down our measurement potential regime to double layer region only to eliminate possible interference from the incomplete reaction/adsorption in a complete CV cycle. Indeed, the measurement in the pure double layer region (0.4-0.6 V vs. RHE) reveals that the conductance shows a flat line, which confirms that there is no more residue redox reaction in this regime, and also further demonstrates the conductance the PtNWs is not sensitive to electrochemical potentials (but only to surface adsorbates). Our results raise question to the conclusion acquired by previous observation on

platinum thin film[30], which is highly possible to be caused by the reaction hysteresis we observe when the sweeping range is broader (**Figure 3-3b**). The ETS measurements in the double regime in a series of solutions with pH values from 0 to 7 show that the ETS signal remains flat for each pH, but with distinct values for different pH (**Figure 3-4a**). Overall, the conductance of PtNWs device is relatively higher in acidic pH (0-3) compared to neutral pH (5-7) and there is a sharp decrease at the pH values in-between. These potential-independent and pH-dependent ETS signals indicate a clear change of surface water structure or protonation status at different pH. What's more, back and forth measurement(**Figure 3-5**) further confirmed that this phenomenon is not caused by the degradation of a device over a lengthy test in multiple solutions.

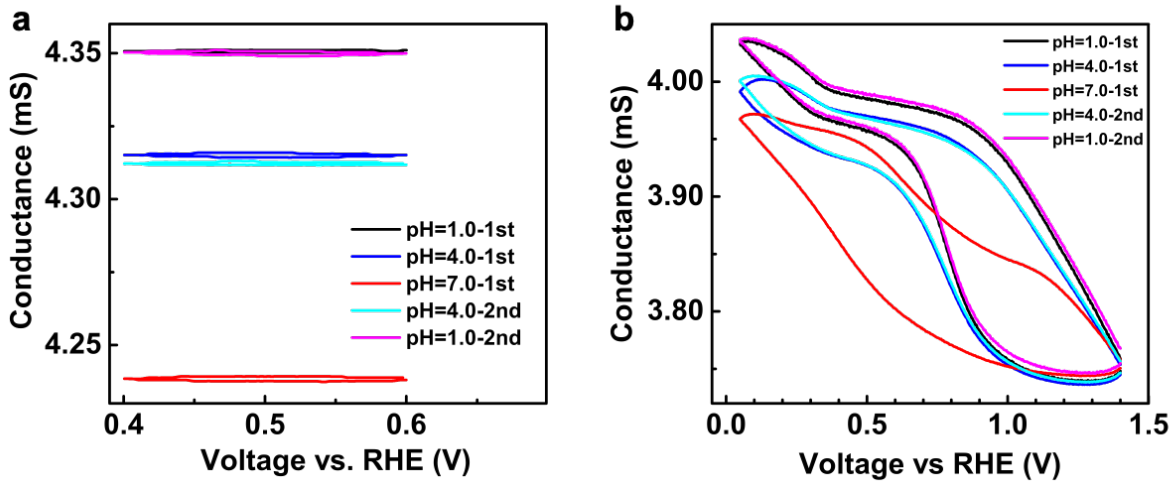

Figure 3-5. Back and forth ETS measurement of hydronium adsorption on Pt surface. (a) Conductance change of a typical PtNW device under controlled potential in double layer region and constant ionic strength (0.10 mol/L). The order of solutions' pH is 1→4→7→4→1. (b) Overall conductance change under the potential of 0.0 V to 1.4 V vs. RHE. Condition is the same as (a).

3.2 Derivation of pKa for surface adsorbed hydronium

The ETS response in the double layer region can be further utilized to obtain quantitative information related to the acidity of the platinum-water interface. By plotting device conductance

versus solution pH (**Figure 3-4b**), we reveal a trend closely resembling protonation/deprotonation of a weak acid. In other words, the nearly constant ETS signal at a high conductance value at pH 1.0-3.0 indicates that there is little change in protonation states of the interfacial water molecules in this pH range, indicating a proton saturated (i.e., 'fully protonated') state. Similarly, a near-constant ETS signal at a low conductance value at pH 5.0-7.0 also indicates that there is little change in protonation states of interfacial water molecules, indicating a fully 'deprotonated' state.

If we assume the Pt-surface hydronium (could be in other forms including $H_5O_2^+$ and $H_9O_4^+$) is a weak acid that may deprotonate like:

$$Pt_x(H_{2y+1}O_y)^+ + H_2O \rightarrow Pt_x(H_2O)_y + H_3O^+ \quad (3\text{-}1)$$

we can write the percentage of protonation as:

$$y = \frac{[HA]}{[HA]+[A^-]} = \frac{1}{1+\frac{Ka}{[H^+]}} = \frac{1}{1+Ka*10^{pH}} \quad (3\text{-}2)$$

If we assume the PtNWs with a fully protonated water surface have a constant conductance of G_p and the PtNWs with a fully deprotonated water surface have a constant conductance of G_{dp}, The ETS conductance signal can be fitted by the equation:

$$G_{conductance} = \frac{G_p - G_{dp}}{1+K_a*10^{pH}} + G_{dp} \quad (3\text{-}3)$$

Importantly, the Henderson–Hasselbalch equation gives a nearly perfect fitting with a pKa of 4.3 and R^2=0.995. This result suggests that hydronium adsorbed on platinum surface is a weaker acid than bulk hydronium, i.e., surface water molecules are expected to be more protonated than bulk water molecules. This is qualitatively consistent with previous theoretical studies that predict a hydronium enrichment near water-Pt interface[27,28]. Previous studies have also indicated the potential of zero charge point show a notable change above pH 3.4(ref. [31]), suggesting a significant change in surface water structure at this point, likely due to a substantial change in protonation status. Compared to these previous studies, our study for the first time provides a quantitative

approach for directly monitoring the surface protonation/deprotonation process to directly determine the surface pKa value.

3.3 Correlation of HER kinetics with surface adsorbed hydronium.

The surface adsorbed hydronium could have important mechanistic consequences for related electrochemical processes including HER or water electrolysis[32]. It has been well documented the HER may show distinct kinetics in different pH, and the exact reason behind such difference is a topic of considerable interest. Indeed, the polarization curves for PtNW catalyzed HER show highly distinct behavior at different pH (**Figure 3-6a**). In particular, when pH is below 4.0, appreciate cathodic HER current can be observed at or below 0 V vs. RHE. On the other hand, when pH is above 4.5, the cathodic HER current observed near 0 V vs. RHE became almost negligible (still discernable in logarithm scale shown in **Figure 3-6b**), and appreciable HER current can only be observed at a much higher overpotential (< -0.2 V vs. RHE). At the intermediate pH (pH 3.0-4.0), a diffusion-limited current plateau occurred, followed by another monotonic increase in reduction current at more negative potential.

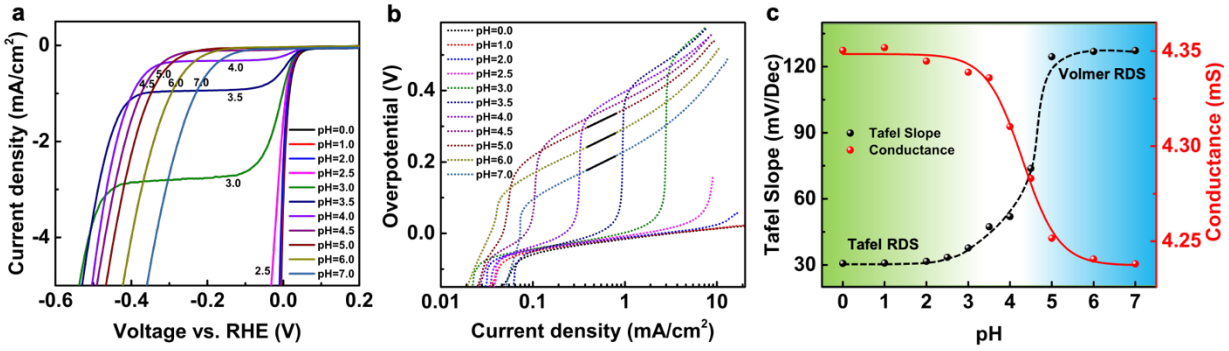

Figure 3-6. Kinetic of hydrogen evolution on Pt. (a) Hydrogen evolution reaction (HER) polarization curves of platinum nanowire on a rotating disk electrode (RDE) in different pH conditions under constant ionic strength (0.10 M). (b) HER current density vs. overpotential plotted in log scale, black solid lines indicate the region where Tafel slope is taken. (c) Tafel slopes measured for the hydrogen evolution reaction in a pH range of 0-7. Regions with different rate-determining step (RDS) are indicated separately. The description of the solution preparation can be found in the method section.

These observations, consistent with previous reports[33], can be explained by two distinct HER reaction pathways resulted from different surface water protonation status, local hydronium concentration and diffusion of hydronium to the surface from the bulk. Based on the logarithmic plot of the polarization curve (**Figure 3-6b**), we can also derive the Tafel slopes for the HER reaction at different pH. For LSV curves with reliable plateau current, we further calibrated the effect of diffusion based on the equation provided by previous mechanism study[34]:

$$\frac{1}{j_{LSV}} = \frac{1}{j_{cat,H^+}} + \frac{1}{j_{plateau}}$$

The curve after calibration (j_{cat,H^+}) and the calibrated Tafel slope are shown in **Figure 3-7** and **Figure 3-6c**. Interestingly, the pH-dependent Tafel slopes also show a sharp transition around pH 4, with a low value of ~30 mV/decade before the transition and a much higher value of ~120 mV/decade after the transition, confirming the distinct reaction pathways.

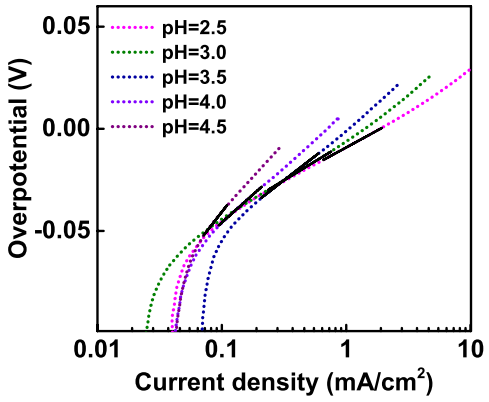

Figure 3-7. Calibrated LSV curve of platinum nanowire, interference of diffusion is eliminated. Black solid line indicates the region where Tafel slope is taken.

It is well recognized that the HER reaction follows three basic steps, with distinct rate-determining steps:

$$H_3O^+ + e^- \rightarrow H_{ad} + H_2O \quad \text{Volmer step} \qquad (3\text{-}4)$$

$$H_{ad} + H_3O^+ + e^- \rightarrow H_2 + H_2O \quad \text{Heyrovsky step} \tag{3-5}$$

$$2H_{ad} \rightarrow H_2 \quad \text{Tafel step} \tag{3-6}$$

in acidic when there is sufficient hydronium; or

$$H_2O + e^- \rightarrow H_{ad} + OH^- \quad \text{Volmer step} \tag{3-7}$$

$$H_{ad} + H_2O + e^- \rightarrow H_2 + OH^- \quad \text{Heyrovsky step} \tag{3-8}$$

$$2H_{ad} \rightarrow H_2 \quad \text{Tafel step} \tag{3-6}$$

in basic conditions when water becomes the major surface species[35]. Based on the assumption that electron-transfer coefficient $\alpha = 0.5$ and a constant surface coverage, the Tafel slope of the reaction would be 30, 40 or 120 mV/dec depending on the rate-determining step being Tafel, Heyrovsky or Volmer step[36, 37].

It is also generally recognized that the Tafel step is the rate-determining in acidic condition, and an ideal Tafel slope of 30 mV/dec is expected. On the other hand, the Volmer step becomes the rate-determining step in a more basic condition, leading to an ideal Tafel slope of 120 mV/dec. Although such distinction reaction mechanism in acidic or basic conditions are well accepted by the community, the transition between these two-reaction mechanisms at intermediate pH is elusive and a topic of considerable debate. Importantly, with our determination of the surface pKa, the change of reaction pathway and the corresponding switch of the Tafel slope can be well explained by the surface protonation status. When the solution pH (0-2) is well below the surface pKa, the surface water is fully protonated, and the reaction follows the acidic pathway way with the Tafel step as the rate-determining step; and when solution pH (5-7) is above surface pKa, the surface water molecules are fully deprotonated, and the Volmer step becomes the rate-determining step. In solution with pH 3-4 which corresponds to the region of a partially protonated surface, the Tafel slope also exhibits a transition, which might be caused by a mix-up of different reaction

mechanisms. However, an accurate Tafel slope cannot be acquired due to the interference of H-upd under this pH condition, which is supported by the observation of H-upd peak at relatively low potential shown in **Figure 3-8**. Additionally, the diffusion-limited current observed in the intermediate pH When pH can be attributed the limited supply of hydronium ions support the first reaction pathway (Tafel limited), which can be confirmed by the linear relationship between plateau current density and hydronium concentration in pH range 2.5-5.

These analyses and the observed mechanism switch demonstrate that surface protonation status dictates the reaction pathway. Future investigation of its relationship with other reaction parameters, e.g. proton transfer barrier, would be very helpful for a better understanding of hydrogen evolution reaction on platinum.

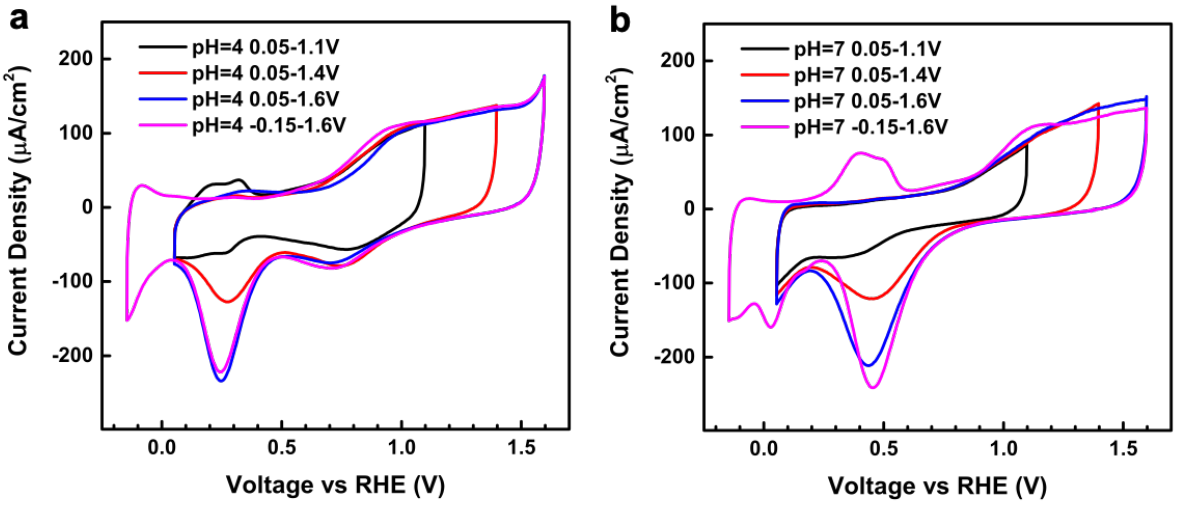

Figure 3-8. Platinum nanowires' cyclic voltammogram with different sweeping range on a rotating disk electrode (RDE) under different pH in unbuffered solution. As shown in the CV curve, the H_{upd} formation starts at a lower potential for near-neutral pH. (a) Results under pH=4.0 condition. (b) Results under pH=7.0 condition.

3.4 ETS characteristic under the potential of hydrogen evolution reaction

Besides information from the double layer region, we are also interested in the pH dependence of PtNWs device's conductivity under the potential of hydrogen evolution reaction (HER). Acquiring such information may provide us with direct evidence of the relationship between surface adsorbed hydronium and HER kinetic. As evident from **Figure 3-9a**, while the conductance change in the D.L. region has the same trend as the results in previous sections, the ETS signal below 0 V vs. RHE exhibit a monotonic decrease between pH value 0.0-6.0. The sudden increase of device conductivity at pH=7.0 is likely to be the result of earlier H_{upd} compared to pH 5.0 and 6.0. ETS measurement in the region of HER (0.1 V to -0.1 V vs. RHE) reveals that conductance change is no longer a flat line due to the reaction hysteresis of rapid adsorption/desorption of hydrogen atoms(**Figure 3-9b**). While the device conductance is higher under lower pH conditions, there is no distinct trend that resembles the observation we had in the double layer region.

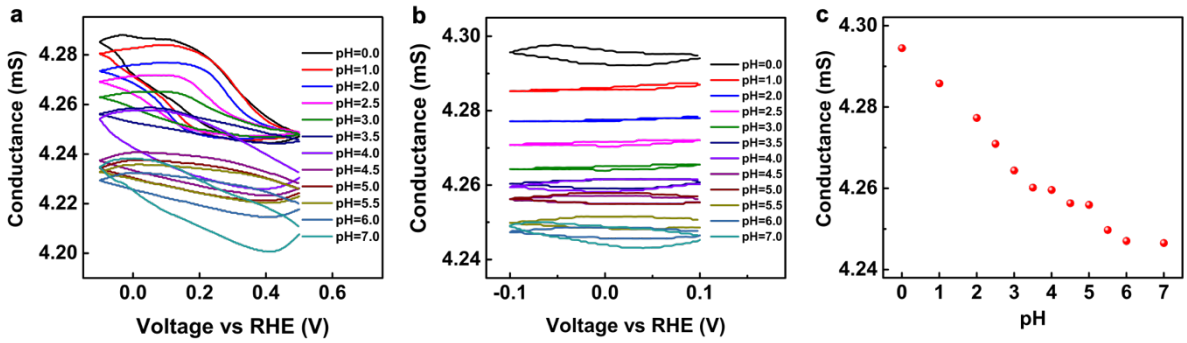

Figure 3-9. In situ electrical transport spectroscopy (ETS) of hydrogen evolution reaction. (a) In-situ conductance vs gate voltage relationship of a typical PtNW device in pH ranging from 0 to 7 under constant ionic strength (0.10 mol/L). (b) ETS measurement at the region of hydrogen evolution reaction. (c) Conductance value extracted from (b).

What's more, the conductance change caused by the adsorption of hydrogen blurred the effect of adsorbed hydronium. As shown in **Figure 3-9a**, when the solution pH is below the surface

pKa (0.0-3.0), increasing pH will results in less adsorbed hydrogen (less conductance increase from double layer region to HER region). However, there is no apparent trend when pH gets higher than the surface pKa. Compared to acidic condition, (pH 0.0-3.0), there is little similarity in the overall variation of surface status when pH is closer to the neutral condition, which is supported by the LSV results in **Figure 3-6** and the CV results in **Figure 3-10b**. Such differences in the onset of hydrogen deposition and hydrogen evolution make it extremely hard for us to compare the ETS response unambiguously, and the conclusion drawn would be less convincing compared to what we have for a clean, water dominant double layer region.

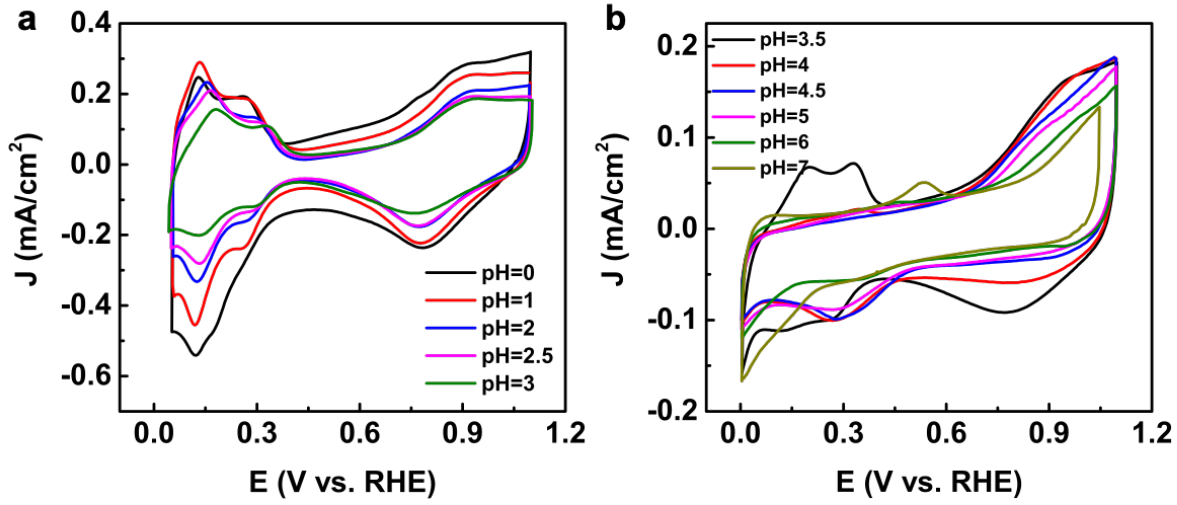

Figure 3-10. CV of platinum nanowires in different unbuffered pH. Results are plotted separately to show the difference between different pH ranges. (a) Results in pH range 0-3. (b) Results in pH range 3.5-7.

4. Conclusion

In summary, with the assistance of electrical transport spectroscopy (ETS), we investigated the acidity of adsorbed protonated species on platinum catalyst surface. Not only qualitative but also quantitative analysis are possible due to the acquirement of highly surface-specific signals under controlled potential range with impeccable precision and accuracy. The platinum-water interface may have different extent of protonation in different pH condition, based on our finding that pKa is ~4.3 for surface adsorbed hydronium. A good correlation between surface protonation and Tafel slope of hydrogen evolution reaction indicates that adsorbed hydronium might be of great importance to specific fundamental electrode surface process. Further work must be done to fully understand the implications of the model presented here on electrocatalysis. What's more, water molecules can act as a base and an acid, which means further deprotonation of the platinum-water interface is highly possible and worth serious examination. Related ETS studies in pH higher than 7 are currently underway.

5. Reference

1. Seh, Z. W.; Kibsgaard, J.; Dickens, C. F.; Chorkendorff, I.; Nørskov, J. K.; Jaramillo, T. F., Combining theory and experiment in electrocatalysis: Insights into materials design. *Science* **2017,** *355* (6321).

2. Stamenkovic, V. R.; Strmcnik, D.; Lopes, P. P.; Markovic, N. M., Energy and fuels from electrochemical interfaces. *Nature Materials* **2017,** *16* (1), 57-69.

3. Li, L.; Wang, P.; Shao, Q.; Huang, X., Metallic nanostructures with low dimensionality for electrochemical water splitting. *Chemical Society Reviews* **2020,** *49* (10), 3072-3106.

4. Mistry, H.; Varela, A. S.; Kühl, S.; Strasser, P.; Cuenya, B. R., Nanostructured electrocatalysts with tunable activity and selectivity. *Nature Reviews Materials* **2016,** *1* (4), 16009.

5. Dubouis, N.; Grimaud, A., The hydrogen evolution reaction: from material to interfacial descriptors. *Chemical Science* **2019,** *10* (40), 9165-9181.

6. Ledezma-Yanez, I.; Wallace, W. D. Z.; Sebastián-Pascual, P.; Climent, V.; Feliu, J. M.; Koper, M. T. M., Interfacial water reorganization as a pH-dependent descriptor of the hydrogen evolution rate on platinum electrodes. *Nature Energy* **2017,** *2* (4), 17031.

7. Velasco-Velez, J.-J.; Wu, C. H.; Pascal, T. A.; Wan, L. F.; Guo, J.; Prendergast, D.; Salmeron, M., The structure of interfacial water on gold electrodes studied by x-ray absorption spectroscopy. *Science* **2014,** *346* (6211), 831-834.

8. Toney, M. F.; Howard, J. N.; Richer, J.; Borges, G. L.; Gordon, J. G.; Melroy, O. R.; Wiesler, D. G.; Yee, D.; Sorensen, L. B., Voltage-dependent ordering of water molecules at an electrode–electrolyte interface. *Nature* **1994,** *368* (6470), 444-446.

9. Iwasita, T.; Xia, X., Adsorption of water at Pt(111) electrode in HClO4 solutions. The potential of zero charge. *Journal of Electroanalytical Chemistry* **1996,** *411* (1), 95-102.

10. Ataka, K.-i.; Yotsuyanagi, T.; Osawa, M., Potential-Dependent Reorientation of Water Molecules at an Electrode/Electrolyte Interface Studied by Surface-Enhanced Infrared Absorption Spectroscopy. *The Journal of Physical Chemistry* **1996,** *100* (25), 10664-10672.

11. Zhang, Y.-J.; Su, Z.-F.; Li, J.-F.; Lipkowski, J., What Vibrational Spectroscopy Tells about Water Structure at the Electrified Palladium–Water Interface. *The Journal of Physical Chemistry C* **2020,** *124* (24), 13240-13248.

12. Gardner, A. M.; Saeed, K. H.; Cowan, A. J., Vibrational sum-frequency generation spectroscopy of electrode surfaces: studying the mechanisms of sustainable fuel generation and utilisation. *Physical Chemistry Chemical Physics* **2019,** *21* (23), 12067-12086.

13. Li, C.-Y.; Le, J.-B.; Wang, Y.-H.; Chen, S.; Yang, Z.-L.; Li, J.-F.; Cheng, J.; Tian, Z.-Q., In situ probing electrified interfacial water structures at atomically flat surfaces. *Nature Materials* **2019,** *18* (7), 697-701.

14. Liu, E.; Jiao, L.; Li, J.; Stracensky, T.; Sun, Q.; Mukerjee, S.; Jia, Q., Interfacial water shuffling the intermediates of hydrogen oxidation and evolution reactions in aqueous media. *Energy & Environmental Science* **2020,** *13* (9), 3064-3074.

15. Darlington, A. M.; Jarisz, T. A.; DeWalt-Kerian, E. L.; Roy, S.; Kim, S.; Azam, M. S.; Hore, D. K.; Gibbs, J. M., Separating the pH-Dependent Behavior of Water in the Stern and Diffuse Layers with Varying Salt Concentration. *The Journal of Physical Chemistry C* **2017,** *121* (37), 20229-20241.

16. Briega-Martos, V.; Herrero, E.; Feliu, J. M., Effect of pH and Water Structure on the Oxygen Reduction Reaction on platinum electrodes. *Electrochimica Acta* **2017,** *241*, 497-509.

17. Wagner, F. T.; Moylan, T. E., Generation of surface hydronium from water and hydrogen coadsorbed on Pt(111). *Surface Science* **1988,** *206* (1), 187-202.

18. Shingaya, Y.; Ito, M., Coordination number and molecular orientation of hydronium cation/bisulfate anion adlayers on Pt(111). *Surface Science* **1996,** *368* (1), 318-323.

19. Hirota, K.; Song, M.-B.; Ito, M., In-situ infrared spectroscopy of water and electrolytes adsorbed on a Pt(111) electrode surface in acid solution. Structural changes of adsorbed water molecules upon an electrode potential. *Chemical Physics Letters* **1996,** *250* (3), 335-341.

20. Dunwell, M.; Yan, Y.; Xu, B., A surface-enhanced infrared absorption spectroscopic study of pH dependent water adsorption on Au. *Surface Science* **2016,** *650*, 51-56.

21. Paredes Olivera, P.; Ferral, A.; Patrito, E. M., Theoretical Investigation of Hydrated Hydronium Ions on Ag(111). *The Journal of Physical Chemistry B* **2001,** *105* (30), 7227-7238.

22. Otani, M.; Hamada, I.; Sugino, O.; Morikawa, Y.; Okamoto, Y.; Ikeshoji, T., Structure of the water/platinum interface—a first principles simulation under bias potential. *Physical Chemistry Chemical Physics* **2008,** *10* (25), 3609-3612.

23. Rossmeisl, J.; Skúlason, E.; Björketun, M. E.; Tripkovic, V.; Nørskov, J. K., Modeling the electrified solid–liquid interface. *Chemical Physics Letters* **2008,** *466* (1), 68-71.

24. Hansen, M. H.; Nilsson, A.; Rossmeisl, J., Modelling pH and potential in dynamic structures of the water/Pt(111) interface on the atomic scale. *Physical Chemistry Chemical Physics* **2017,** *19* (34), 23505-23514.

25. Rice, P. S.; Mao, Y.; Guo, C.; Hu, P., Interconversion of hydrated protons at the interface between liquid water and platinum. *Physical Chemistry Chemical Physics* **2019,** *21* (11), 5932-5940.

26. Buch, V.; Milet, A.; Vácha, R.; Jungwirth, P.; Devlin, J. P., Water surface is acidic. *Proceedings of the National Academy of Sciences* **2007,** *104* (18), 7342-7347.

27. Limmer, D. T.; Willard, A. P.; Madden, P.; Chandler, D., Hydration of metal surfaces can be dynamically heterogeneous and hydrophobic. *Proceedings of the National Academy of Sciences* **2013,** *110* (11), 4200-4205.

28. Brüesch, P.; Christen, T., The electric double layer at a metal electrode in pure water. *Journal of Applied Physics* **2004,** *95* (5), 2846-2856.

29. Liao, L. W.; Li, M. F.; Kang, J.; Chen, D.; Chen, Y.-X.; Ye, S., Electrode reaction induced pH change at the Pt electrode/electrolyte interface and its impact on electrode processes. *Journal of Electroanalytical Chemistry* **2013,** *688*, 207-215.

30. Fujihara, M.; Kuwana, T., Studies of electrochemical interfaces of thin PT film electrodes by surface conductance. *Electrochimica Acta* **1975,** *20* (8), 565-573.

31. Rizo, R.; Sitta, E.; Herrero, E.; Climent, V.; Feliu, J. M., Towards the understanding of the interfacial pH scale at Pt(111) electrodes. *Electrochimica Acta* **2015,** *162*, 138-145.

32. Kim, Y.; Noh, C.; Jung, Y.; Kang, H., The Nature of Hydrated Protons on Platinum Surfaces. *Chemistry – A European Journal* **2017,** *23* (69), 17566-17575.

33. Shinagawa, T.; Garcia-Esparza, A. T.; Takanabe, K., Mechanistic Switching by Hydronium Ion Activity for Hydrogen Evolution and Oxidation over Polycrystalline Platinum Disk and Platinum/Carbon Electrodes. *ChemElectroChem* **2014,** *1* (9), 1497-1507.

34. Galvez-Vazquez, M. d. J.; Grozovski, V.; Kovacs, N.; Broekmann, P.; Vesztergom, S., Full model for the two-step polarization curves of hydrogen evolution, measured on RDEs in dilute acid solutions. *The Journal of Physical Chemistry C* **2020,** *124* (7), 3988-4000.

35. Banta, M. C.; Hackerman, N., The Effect of Acidity on the Differential Capacity of Polarized Platinum Electrodes. *Journal of The Electrochemical Society* **1964,** *111* (1), 114.

36. Marković, N. M.; Grgur, B. N.; Ross, P. N., Temperature-Dependent Hydrogen Electrochemistry on Platinum Low-Index Single-Crystal Surfaces in Acid Solutions. *The Journal of Physical Chemistry B* **1997,** *101* (27), 5405-5413.

37. Conway, B. E.; Bai, L., Determination of adsorption of OPD H species in the cathodic hydrogen evolution reaction at Pt in relation to electrocatalysis. *Journal of Electroanalytical Chemistry and Interfacial Electrochemistry* **1986,** *198* (1), 149-175.

Chapter 4. Sensing application of electrical transport spectroscopy (ETS)

1. Introduction and background

The ability to selectively and rapidly detect DNA and other large biomolecules at extremely low concentration is essential to many fields including clinical diagnostics, environmental monitoring and forensic analysis[1-4]. Based on different sensing mechanism, various techniques have been developed for DNA sensing. The majority of the DNA sensors are based on the event of DNA hybridization and the following signal produced, which could be electrochemical signal, electrical signal, optical signal and mechanical/piezoelectric signal[5-8]. However, most of the DNA sensing system requires the introduction of labels, such as electrochemical active species like methylene blue (MB) or fluorescence species. In order to further decrease the time and cost for DNA sensing techniques, label-free detection, with a simplified sample preparation procedure, is a very appealing solution.

Among the mechanisms that are suitable for label-free detection of DNA, sensing the electrical signal caused by the presence of the target molecule is most promising. Such devices often bear the feature of a field-effect transistor (FET), which does not require special modification to the target analyte for signal amplification. Biosensors with FET configuration are receiving more and more consideration over the past decades, due to the ultra-high sensitivity (ng to pg per mL) they can achieve and the abundance of material to choose from[9-12]. What's more, the binding interactions include protein-protein interaction, DNA hybridization and ligand-receptor interaction. FET biosensor has been thoroughly reviewed previously[13, 14]. Limited by space, we will mainly focus on the drawbacks of this type of method that need to be addressed before commercialization. Besides the difficulty of mass production and poor reproducibility, the biggest challenge is the charge screening effect at the double layer.

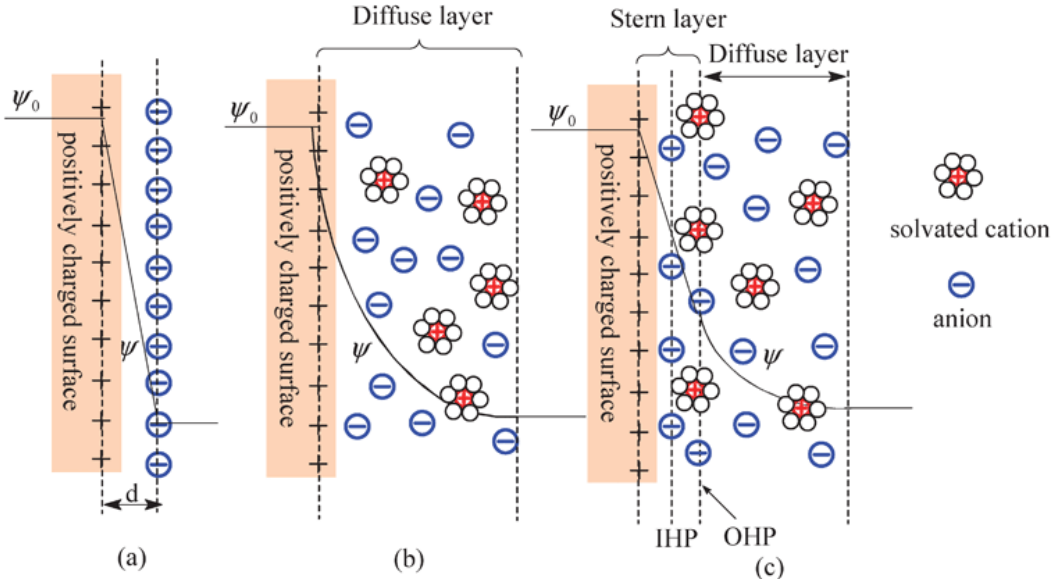

Figure 4-1. Schematic representations of different model for electrical double layer structure. (a) the Helmholtz model. (b) the Gouy–Chapman model. (c) the Gouy–Chapman–Stern model. Adapted from reference 14 with copyright permission.

Starting from the most simple Helmholtz model, the model of electrical double layer evolved with the development of physics and electrochemistry (**Figure 4-1**)[15-17]. The most widely accepted model is the Gouy–Chapman–Stern model (**Figure 4-1c**), which includes the Stern layer consisting of inner/outer Helmholtz planes (IHP/OHP) and the diffuse layer with a thickness known as Debye length λ_D. Debye length represents the distance from OHP to a depth in the solution where the surface electrostatic effect can affect ions presenting. Such screening effect would considerably affect the detection limit for biomolecules with electrostatic charges (i.e. DNA and protein), as shown in **Figure 4-2**.

The equation to calculate Debye length is:

$$\lambda_D = \sqrt{\frac{\varepsilon_0 \varepsilon_r kT}{2N_A q^2 I}}$$

Where ε_0 is the permittivity of free space, ε_r is the dielectric constant of the solution, N_A is Avogadro's number, k is Boltzmann constant and I the ionic strength. As shown in the equation, a solution with low ionic strength will exhibit a large Debye length and less double layer screening[18]. Thus, a delicate balance between Debye length and the binding distance of the target analyte is essential to achieve best sensitivity.

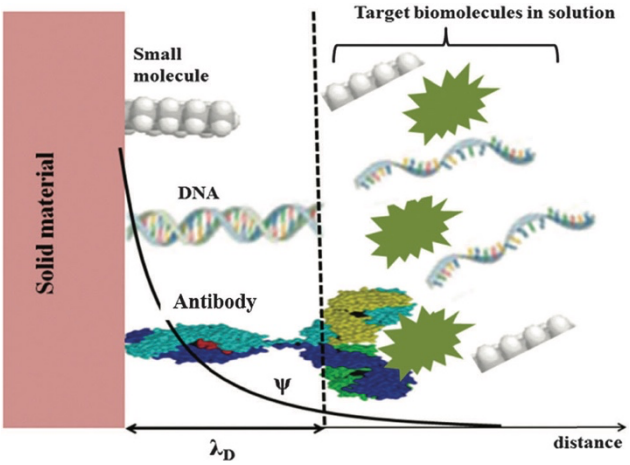

Figure 4-2. Schematic representation of Debye screening of different biomolecules with different binding mechanism. The detection of biomolecule needs to occur at a distance smaller than Debye length λ_D. Adapted from reference 14 with copyright permission.

The structure of DNA molecules resembles a circular cylinder with ~2 nm diameter, while each nucleotide can contribute 0.34 nm to the height of the cylinder[19, 20]. The negative charge brought by the phosphate backbone of DNA is largely screened by the double layer, especially in biological environments (i.e. an extracted bio-sample) where the Debye length is very short (usually smaller than 1 nm), making the detection extremely difficult. Besides the strategy of decreasing ionic strength of the electrolyte, other solutions include the attachment of a biomolecule permeable polymer layer[21] and the implementation of high-frequency measurement[22].

As introduced in the previous chapters, the electrical transport spectroscopy (ETS) developed by our group can serve as a suitable on-chip signaling technique for in situ studies of electrode/electrolyte interface. Since it is based on the scattering effect of the species closest to the

surface (from the inner Helmholtz plane), it is not affected by the screening effect of the double layer. The surface pKa investigation presented in the previous chapter verified the ability for ETS to detect the interference of surface water structure by near-surface species originated from the bulk solution. If the charged DNA molecules could have a similar effect on the interfacial water, we might be able to achieve highly sensitive detection without worrying about the Debye screening in a biological environment with high ionic strength. The schematic illustration of the experimental procedure and detection mechanism is shown in **Figure 4-3,** which will be described in detail in the following sections. Here in this chapter, we explore the ETS configuration's potential in the field of label-free molecular sensing. We achieved successful detection of hydrogen peroxide by designing controlled experiments under different pH conditions. At last, we examined the feasibility of the DNA sensing mechanism mentioned previously.

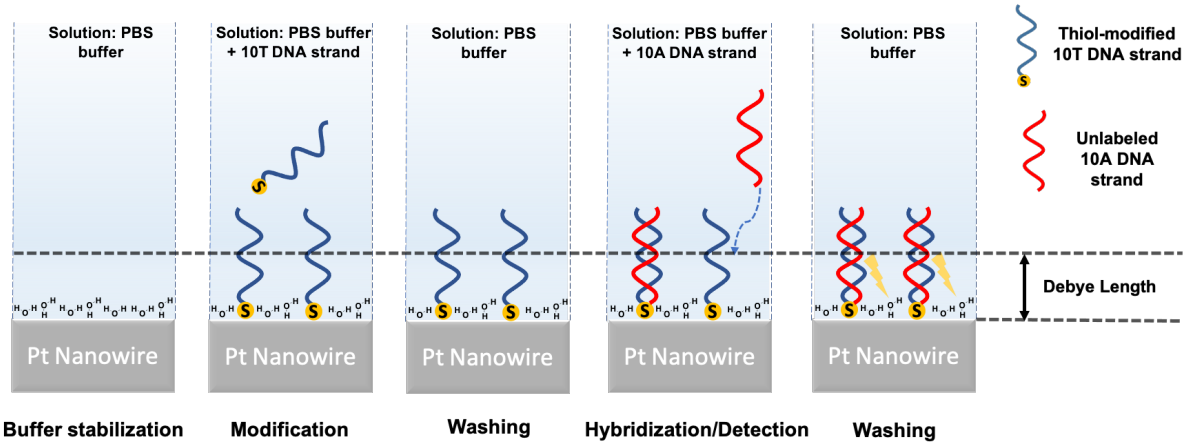

Figure 4-3. Schematic representation of DNA sensing based on ETS configuration. The species near the platinum-water interface are shown for different steps of the measurement (cations and anions existing in phosphate buffer solution (PBS) are emitted here for clearness of the figure). The yellow flash symbol represents the charge effect towards the inner Helmholtz plane's structure caused by DNA molecules after hybridization.

2. Materials and methods

2.1 Modification of platinum nanowire device with DNA

The process of preparing PtNW devices is the same as described in previous chapters. In order to detect the target single-stranded DNA molecule, we need to first modify our device surface with the complementary DNA. Modification of gold surface with thiol-ended molecule is extensively investigated due to the development in molecular electronic devices. The high stability of the alkanethiol's self-assembled monolayers (SAMs) ensured its application in the fields including anti-corrosion, wetting and molecular sensing[23, 24]. More recently, increased attention was paid to the preparation of SAM on other metal surfaces including Pt, Cu and Ni[25]. In order to achieve the best quality of the SAM on platinum, two approaches are developed to avoid/eliminate surface oxidation: by minimizing exposure to oxygen or by mechanical cleaning.

The microfluidic system we developed is perfect for the surface modification procedure with minimized oxygen exposure. Owing to the fact that the PtNW device is always covered with a degassed solution inside the microfluidic chamber. Another huge advantage of the microfluidic system means we only need a small amount of solution for surface modification, which is a lot more economically efficient. What's more, we can easily monitor the process of surface modification by monitoring the conductance change of the device. Compared to water molecules, the adsorption of the sulfur atom will result in a stronger scattering effect thus a lower device conductivity. Measuring the conductance-time relationship can provide us information about the completion of surface modification, which will be discussed in detail in the result section.

2.2 On-chip electrical transport spectroscopy (ETS) measurements for DNA detection

A two-channel source-measure unit (SMU, Keysight B2902a) was used for the activation of PtNWs device with the condition described in the previous chapters. No gate voltage control is

need since the conductance change is enough to reflect the change of interfacial structure. After the activation process, the clean platinum nanowire device is exposed to a degassed phosphate buffer solution (PBS, 0.1 mol/L) followed by a buffer containing (1 μmol/L) of thiol-terminated DNA molecules (**Figure 4-3**). Before and after the DNA hybridization event, the microfluidic chamber was flushed with buffer solution. By applying a constant source-drain voltage (10 mV), the current-time relationship was monitored throughout the entire testing process. The typical flow rate was 2 $mL \cdot h^{-1}$ during electrolyte switching. All solutions were degassed with ultrahigh purity nitrogen before use.

3. Results and discussion

3.1 Hydrogen peroxide sensing of platinum nanowire device

Before the implementation of ETS for DNA sensing, we need to examine is the PtNW device is sensitive to the charged species near the surface (e.g. H^+) or chemical processes that consume specific charged species near the surface. Hydrogen peroxide is a good target molecule. In our previous publication[26], the reduction and oxidation of H_2O_2 were investigated with ETS. The reduction reaction for hydrogen peroxide is:

$$H_2O_2 + 2H^+ + 2e^- \rightarrow 2H_2O$$

Where hydronium is consumed at the same time. Such consumption wouldn't cause an obvious change in near-surface H^+ concentration in acidic condition, but the situation would be different when hydronium concentration is relatively low. Thus, the ETS curve should have little variation in acidic condition when a low concentration of H_2O_2 is introduced. **Figure 4-4a** shows typical ETS baseline features and the ETS with 1 μM of H_2O_2 added to $HClO_4$ solution. Obviously, there is little difference between these two curves.

The situation is indeed different when the solution environment contains limited amount of hydronium, as shown in **Figure 4-4b**. When a low concentration of hydrogen peroxide is presenting in a solution with pH=7 (0.1mol/L $KClO_4$), a distinct variation of the ETS signal can be observed. The most obvious change happens near the region of hydrogen adsorption. For pH 7 the oxide reduction and hydrogen adsorption in the backward scan are not well separated, which is supported by the CV measurement in the previous chapter. The existence of hydrogen peroxide resulted in competitive consumption of near-surface hydronium when it is being reduced. Thus less hydrogen would adsorb onto the platinum surface and less change observed for the hydrogen region. Back and forth measurement further confirms that this observation is reproducible and is not caused by the degradation of PtNWs device over different solution. What's more, a higher concentration of H_2O_2 would result in a larger change in H-upd region, which proves the capability of molecular sensing based on detection of near-surface species variation. Last but not least, the concentration we are using here is already low enough for practical application (μM level)[27].

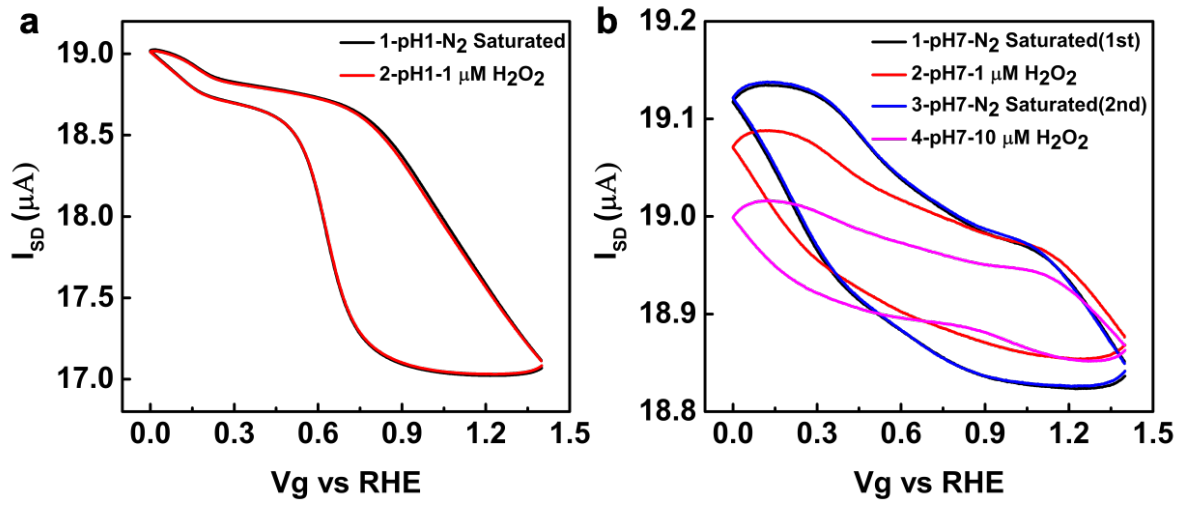

Figure 4-4. In situ electrical transport spectroscopy (ETS) of hydrogen peroxide sensing on Pt surface. (a) I_{SD}–V_G (ETS) characteristics of a typical PtNW device in 0.1 M HClO4 (black) and with the addition of low concentration of H_2O_2. (b) ETS characteristics in neutral (pH=7) condition, with and without the introduction of H_2O_2.

3.2 DNA sensing of PtNW device

After a successful attempt of hydrogen peroxide detection, we moved on to verify the capability of ETS in DNA sensing. Following the procedure illustrated in **Figure 4-3**, we monitored the current-time relationship over the entire process. As shown in **Figure 4-5**, the device exhibits a distinct response to the solution in the microfluidic chamber. Right after the activation in perchloric acid, DI water was introduced to wash away the remaining acid. As expected, a decrease in I_{SD} was observed due to the deprotonation of the platinum surface. The introduction of phosphate buffer after DI water results in another decrease in device conductance, probably due to the adsorption of phosphoric anion on PtNWs device.

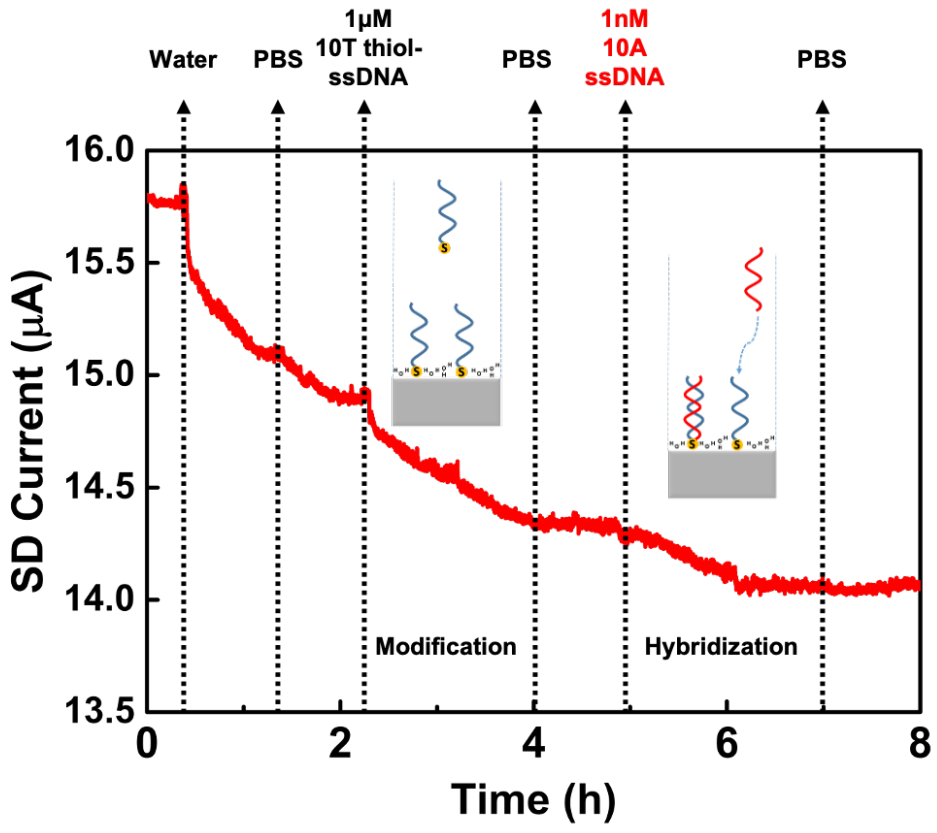

Figure 4-5. Response of a typical PtNW device during modification and followed-up DNA hybridization. Every solution switch is highlighted by the dashed line and the type of solution above. The measurement was initiated right after activation in perchloric acid.

After stabilization of observed current, PBS containing 1 μM of thiol-terminated 10T DNA strand was drawn into the system. The modification process usually takes 2 hours to complete, as shown by the stabilized current in **Figure 4-5**. To remove the interference of unattached 10T DNA in solution, phosphate buffer was drawn through the chamber continuously for another 30 minutes. An unchanging current indicates the stability of the device and the thiol modification. After this, a buffered solution containing the complementary 10A DNA (1 nmol/L) strand was introduced for hybridization/detection. As shown in **Figure 4-5**, a further decrease in device conductance can be observed. This observation is caused by the 10A DNA molecule, and another test without surface modification (**Figure 4-6**) confirmed that it is the event of hybridization between complementary 10T and 10A DNA that leads to the decrease of I_{SD}.

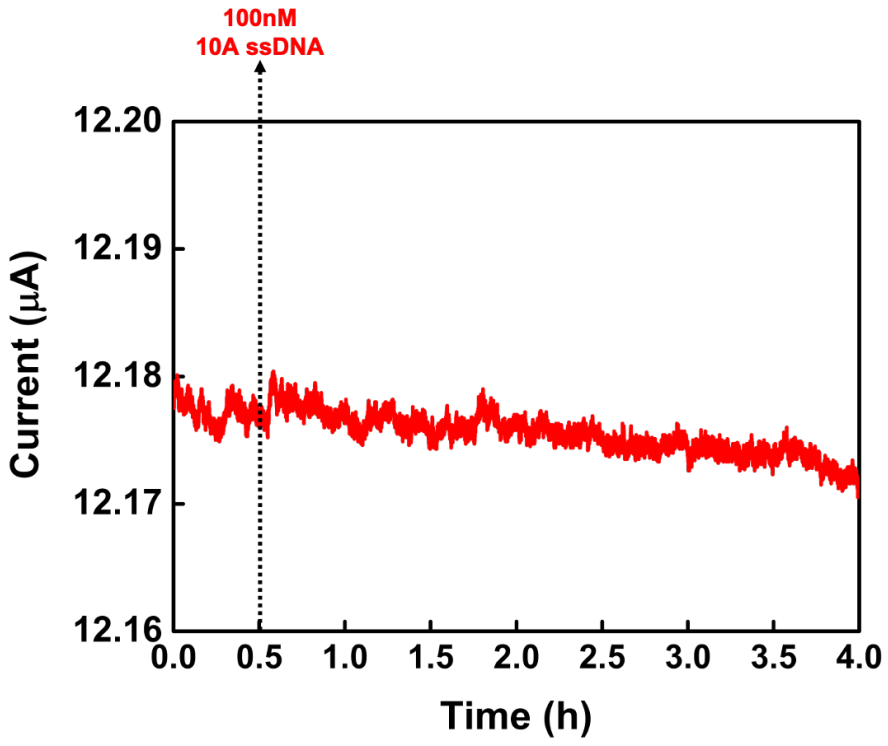

Figure 4-6. Typical response of PtNW device without functionalization of thiol-terminated 10T DNA, no obvious response was detected. All solutions are prepared based on phosphate buffer solution.

Notably, the successful detection of 1nM 10T DNA was achieved at a buffer solution with relatively high ionic strength, which means the scenario we anticipated at the beginning of this chapter is possible. The highly surface-sensitive nature of ETS measurement ensured real-time detection that overcame the challenge of double layer screening. Even though, there are still several limitations to the current system we are using. First, the detection limit is not low enough compared to state of art DNA sensors (pM to fM detection limit)[28]. The signal-to-noise ratio would be unacceptable if we need to detect pM level of DNA strand. Second, similar to other FET-based DNA sensor, the reproducibility of our measurement is not ideal, which is mainly due to the difference between the PtNW devices. Even though they are fabricated with the same PtNWs thin film, the distribution of the nanowire network is not totally identical between themselves. This would make it extremely difficult to acquire a reliable relationship between the target analyte's concentration and device response. Further improvements to the current configuration should focus mainly on lowering the noise level and improving reproducibility.

4. Conclusion

In conclusion, we have shown that with specific modification, the electric transport spectroscopy can probe distinct conductance signatures upon hybridization of complementary single-strand DNA. Successful detection of nM level of DNA was achieved in solution with high ionic strength, which means the proposed mechanism of sensing without the limit of double layer screening is possible. This sensor showed many advantages, including simplicity, selectivity and good stability. It should be pointed out that the reproducibility and signal-to-noise ratio can be further improved. What's more, we have also investigated the ETS system's potential for hydrogen peroxide sensing. Further research in this direction should focus mainly on improving the detection limit of the current ETS configuration.

5. Reference

1. Ligler, F. S.; Erickson, J. S., Diagnosis on disc. *Nature* **2006,** *440* (7081), 159-160.

2. Janasek, D.; Franzke, J.; Manz, A., Scaling and the design of miniaturized chemical-analysis systems. *Nature* **2006,** *442* (7101), 374-380.

3. Liu, P.; Li, X.; Greenspoon, S. A.; Scherer, J. R.; Mathies, R. A., Integrated DNA purification, PCR, sample cleanup, and capillary electrophoresis microchip for forensic human identification. *Lab on a Chip* **2011,** *11* (6), 1041-1048.

4. Liu, H.; Xu, S.; He, Z.; Deng, A.; Zhu, J.-J., Supersandwich cytosensor for selective and ultrasensitive detection of cancer cells using aptamer-DNA concatamer-quantum dots probes. *Analytical chemistry* **2013,** *85* (6), 3385-3392.

5. Wang, D.; Hu, L.; Zhou, H.; Abdel-Halim, E.; Zhu, J.-J., Molecular beacon structure mediated rolling circle amplification for ultrasensitive electrochemical detection of microRNA based on quantum dots tagging. *Electrochemistry communications* **2013,** *33*, 80-83.

6. Ma, Z.; Tian, L.; Wang, T.; Wang, C., Optical DNA detection based on gold nanorods aggregation. *Analytica chimica acta* **2010,** *673* (2), 179-184.

7. Rashid, J. I. A.; Yusof, N. A., The strategies of DNA immobilization and hybridization detection mechanism in the construction of electrochemical DNA sensor: A review. *Sensing and bio-sensing research* **2017,** *16*, 19-31.

8. Chen, A.; Chatterjee, S., Nanomaterials based electrochemical sensors for biomedical applications. *Chemical Society Reviews* **2013,** *42* (12), 5425-5438.

9. Hakim, M. M.; Lombardini, M.; Sun, K.; Giustiniano, F.; Roach, P. L.; Davies, D. E.; Howarth, P. H.; de Planque, M. R.; Morgan, H.; Ashburn, P., Thin film polycrystalline silicon nanowire biosensors. *Nano letters* **2012,** *12* (4), 1868-1872.

10. Cheng, Y.; Chen, K.-S.; Meyer, N. L.; Yuan, J.; Hirst, L. S.; Chase, P. B.; Xiong, P., Functionalized SnO2 nanobelt field-effect transistor sensors for label-free detection of cardiac troponin. *Biosensors and Bioelectronics* **2011,** *26* (11), 4538-4544.

11. Allen, B. L.; Kichambare, P. D.; Star, A., Carbon nanotube field-effect-transistor-based biosensors. *Advanced Materials* **2007,** *19* (11), 1439-1451.

12. Park, S. J.; Kwon, O. S.; Lee, S. H.; Song, H. S.; Park, T. H.; Jang, J., Ultrasensitive flexible graphene based field-effect transistor (FET)-type bioelectronic nose. *Nano letters* **2012,** *12* (10), 5082-5090.

13. Mehrabani, S.; Maker, A. J.; Armani, A. M., Hybrid integrated label-free chemical and biological sensors. *Sensors* **2014,** *14* (4), 5890-5928.

14. Huang, W.; Diallo, A. K.; Dailey, J. L.; Besar, K.; Katz, H. E., Electrochemical processes and mechanistic aspects of field-effect sensors for biomolecules. *Journal of Materials Chemistry C* **2015,** *3* (25), 6445-6470.

15. Zhang, L. L.; Zhao, X., Carbon-based materials as supercapacitor electrodes. *Chemical Society Reviews* **2009,** *38* (9), 2520-2531.

16. Helmholtz, H. v., Ueber einige Gesetze der Vertheilung elektrischer Ströme in körperlichen Leitern, mit Anwendung auf die thierisch-elektrischen Versuche (Schluss.). *Annalen der Physik* **1853,** *165* (7), 353-377.

17. Gouy, M., Sur la constitution de la charge électrique à la surface d'un électrolyte. *J. Phys. Theor. Appl.* **1910,** *9* (1), 457-468.

18. Stern, E.; Wagner, R.; Sigworth, F. J.; Breaker, R.; Fahmy, T. M.; Reed, M. A., Importance of the Debye screening length on nanowire field effect transistor sensors. *Nano letters* **2007,** *7* (11), 3405-3409.

19. Piunno, P. A.; Watterson, J.; Wust, C. C.; Krull, U. J., Considerations for the quantitative transduction of hybridization of immobilized DNA. *Analytica chimica acta* **1999,** *400* (1-3), 73-89.

20. Schöning, M. J.; Poghossian, A., Recent advances in biologically sensitive field-effect transistors (BioFETs). *Analyst* **2002,** *127* (9), 1137-1151.

21. Gao, N.; Zhou, W.; Jiang, X.; Hong, G.; Fu, T.-M.; Lieber, C. M., General strategy for biodetection in high ionic strength solutions using transistor-based nanoelectronic sensors. *Nano letters* **2015,** *15* (3), 2143-2148.

22. Kulkarni, G. S.; Zhong, Z., Detection beyond the Debye screening length in a high-frequency nanoelectronic biosensor. *Nano letters* **2012,** *12* (2), 719-723.

23. Bain, C. D.; Troughton, E. B.; Tao, Y. T.; Evall, J.; Whitesides, G. M.; Nuzzo, R. G., Formation of monolayer films by the spontaneous assembly of organic thiols from solution onto gold. *Journal of the American Chemical Society* **1989,** *111* (1), 321-335.

24. Tour, J. M., Molecular electronics. Synthesis and testing of components. *Accounts of Chemical Research* **2000,** *33* (11), 791-804.

25. Petrovykh, D. Y.; Kimura-Suda, H.; Opdahl, A.; Richter, L. J.; Tarlov, M. J.; Whitman, L. J., Alkanethiols on platinum: Multicomponent self-assembled monolayers. *Langmuir* **2006,** *22* (6), 2578-2587.

26. Ding, M.; He, Q.; Wang, G.; Cheng, H.-C.; Huang, Y.; Duan, X., An on-chip electrical transport spectroscopy approach for in situ monitoring electrochemical interfaces. *Nature Communications* **2015,** *6*, 7867.

27. Meier, J.; M Hofferber, E.; A Stapleton, J.; M Iverson, N., Hydrogen peroxide sensors for biomedical applications. *Chemosensors* **2019,** *7* (4), 64.

28. Baig, M. M. F. A.; Lai, W.-F.; Akhtar, M. F.; Saleem, A.; Ahmed, S. A.; Xia, X.-H., DNA nanotechnology as a tool to develop molecular tension probes for bio-sensing and bio-imaging applications: An up-to-date review. *Nano-Structures & Nano-Objects* **2020,** *23*, 100523.

Chapter 5. Conclusion

There are many practically important processes happening at the electrode/electrolyte interfaces. Tremendous effort was devoted to developing a better understanding of the geometric, electronic, and molecular structure of the interface. Due to limited understanding of the interface, the debate and cross-corroboration between results from different characterization techniques will continue for a period of time.

In conclusion, with the novel on-chip ETS approach developed by our group, we can gather important information from the catalyst-solution interface and relates it to the crucial reaction process. We investigated in anion (Cl^-, Br^-, I^-, SO_4^{2-}) adsorption on platinum catalyst's surface. Due to the abundance of halide in natural and industrial environments, the mechanistic study of the halide adsorption (especially in trace amount) on Pt catalysts is of both fundamental and practical significance. The results of halide anionic adsorption on the PtNWs in halide containing electrolytes proves that ETS can carry out qualitative and quantitative analysis at low concentration of target analyte. We further investigated the chloride poisoning behavior in more complex anionic environments and demonstrate potential strategies to mitigate the poisoning effect using either a "static" anionic cyanide adlayer (that could hinder Cl^- adsorption and reduce the Cl_{ads} induced overpotential) or a "dynamic" high ionic strength approach (that helps prevent the long-term accumulation of Cl^- poisoning) for improved efficiency and stability of practical energy devices.

Take a step forward, we investigated the pH effect towards the structure of electrical double layer. The unique signaling pathway of ETS ensured its high sensitivity to trivial change at the interface. The platinum-water interface may have different extents of protonation in different pH conditions, based on our finding that pKa is ~4.3 for surface adsorbed hydronium. The results from

Reactive force field simulation and AIMD simulation provide crucial support of hydronium ion's acidity and its influence on the interfacial structure, which will be included together in the publication in progress. A good correlation between surface protonation and Tafel slope of hydrogen evolution reaction indicates that adsorbed hydronium might be of great importance to specific fundamental electrode surface process. Further work must be done to fully understand the implications of the model presented here on electrocatalysis. What's more, a water molecule can act as a base and an acid, which means further deprotonation of the platinum-water interface is highly possible and worth serious examination.

At last, we modified the platinum nanowire device and utilized it to probe distinct conductance signatures upon hybridization of complementary single-strand DNA. Successful detection of nM level of DNA was achieved in solution with high ionic strength, which means the proposed mechanism of sensing without the limit of double layer screening is possible. This sensor showed many advantages, including simplicity, selectivity and good stability. What's more, we have also investigated the ETS system's potential for hydrogen peroxide sensing.

As for the future of ETS characterization, there are still many potential directions to explore. The cation effect in basic condition and its relationship with specific reactions (e.g. HER and ORR) is one example. Besides, how surface modification may affect the interfacial structure is also worthy to be investigated. Furthermore, the coupling of traditional electrochemical methods such as voltammetry offers the capability of extending this system to a wide range of interdisciplinary research fields (biological materials/systems) where electrochemical process plays a central role.